A MULTI-PROXY RECONSTRUCTION OF ENVIRONMENTAL CHANGE IN THE VICINITY OF THE NORTH BAY OUTLET OF PRO-GLACIAL LAKE ALGONQUIN

[1]Ryan J. Rabett*, [2]Alexander J.E. Pryor, [1]David J. Simpson, [3]Lucy R. Farr, [1]Sean Pyne-O'Donnell, [1]Maarten Blaauw, [4]Simon Crowhurst, [5]Riley P.M. Mulligan, [6]Christopher O. Hunt, [7]Rhiannon Stevens, [6]Marta Fiacconi, [3]David Beresford-Jones, [8]Paul F. Karrow

[1] School of Natural & Built Environment, Queen's University Belfast, Elmwood Avenue, Belfast BT7 1NN, UK.
[2] Department of Archaeology, University of Exeter, Laver Building, North Park Road, Streatham Campus, Exeter EX4 4QE, UK.
[3] McDonald Institute for Archaeological Research, University of Cambridge, Downing Street, Cambridge CB2 3ER, UK.
[4] Department of Earth Sciences, University of Cambridge, Downing Street, Cambridge CB2 3EQ, UK.
[5] Ontario Geological Survey, 933 Ramsey Lake Road, Sudbury, Ontario P3E 6B5, Canada.
[6] Natural Sciences & Psychology, Liverpool John Moores University, James Parsons Building, Byrom Street Liverpool L3 3AF, UK.
[7] Institute of Archaeology, University College London, 31-34 Gordon Square, London WC1H 0PY, UK.
[8]Department of Earth & Environmental Sciences, Centre for Environmental and Information Technology (EIT), University of Waterloo, 200 University Ave. W, Waterloo, Ontario N2L 3G1, Canada.

*Corresponding author

ABSTRACT

We present a multi-proxy study of environmental conditions during and after the recessional phases of pro-glacial Lake Algonquin in the vicinity of the North Bay outlet, Great Lakes Basin. Data presented comes from a new sedimentary profile obtained from the Balsam Creek kettle lake c. *34km north-east of the city of North Bay. This site lay close to the northeast margin of the maximum extent of the post-Algonquin lake sequence, which drained through the Ottawa-Mattawa valley system. Our data are presented against a Bayesian age-depth model, supporting and extending regional understanding of vegetation succession in this part of north-east Ontario. The core profile provides a minimum age for the formation of the glacial outwash delta in which the kettle is set, as well as a tentative timing for the Payette (post-Algonquin) lake phase. We highlight two discrete intervals during the Early Holocene, with modelled mean ages of: 8475-8040 cal. BP (332-316cm) and 7645 cal. BP (286cm), when climatic aridity affected the growth of vegetation within the kettle vicinity. Association with volcanic activity is posited. Cryptotephra dating to 7660-7430 cal. BP (mean age: 7580 cal. BP) is chronologically and geochemically assigned to the Mazama climactic eruption, while an earlier ash accumulation 8710-7865 cal. BP is tentatively sourced to an unknown eruption also in the Cascades region of Oregon. Outside of these periods, the Balsam Creek sequence shows considerable habitat stability and a character akin to that seen at more southerly latitudes. On this evidence we propose that access to reliable resources within kettle features could have aided the initial colonisation of northern Ontario's environmentally dynamic early post-glacial landscape.*

Keywords: Lake Algonquin, post-glacial, kettle lake, multi-proxy, climate, cryptotephra, colonisation

1. INTRODUCTION

The sequence of pro-glacial lakes that formed in front of the decaying Laurentide ice-sheet have been a subject of study since the late nineteenth century (Spencer 1891) when the evidence for continental glaciation became widely accepted, and supported by the documentation of tilted shorelines in all of the Great Lakes basins. Although work tended to progress piecemeal because of the complexity of the evidence and its distribution over such a large area, the increasingly detailed story was first drawn together in a large monograph by Leverett and Taylor (1915); an account that would stand for decades as the reference work on Great Lakes history (*see* Kehew & Brandon Curry 2018). It would not be until the 1950s that palynological studies of vegetation and climate change were undertaken by the Geological Survey of Canada across the country. In the North Bay area work by Jaan Terasmae in particular determined the outflow from pro-glacial Lake Algonquin to have occurred *c*. 10,000 ^{14}C yr BP (Terasmae & Hughes 1960). A glacial retreat history that became the standard reference for this part of the region was later developed by Saarnisto (1974), based on palynological records from several lakes east of Lake Superior. Subsequently, such studies became more commonly used as a way of tracking post-glacial vegetation succession (*see* summary in Bryant & Holloway 1985). Between the 1960s and 1980s the Quaternary geology of southern Ontario was comprehensively covered. To the north, however, on the Canadian Shield (and the area of the present study), mapping was more restricted to drift prospecting areas in support of mining development. Three urban areas in the east-west lowlands were mapped: North Bay (Harrison, 1972), Sudbury (Burwasser 1979; Barnett & Bajc 2002) and Sault Ste. Marie (Cowan & Broster, 1988). North Bay was given notable attention because of its proximity to the Lake Algonquin outlet. It would be the completion of country-wide coverage by aerial photographs after the Second World War that proved crucial to the reconnaissance mapping by Boissonneau (1968) of the soils and geomorphic features of the large area from Lake Superior to the Quebec border and from Lake Huron north to latitude 48° 30′. In that work he delineated nine east-west sub-parallel terminal moraines in the central part of the area west of Sudbury and roughed out the extent of pro-glacial lakes Barlow-Ojibway and Algonquin.

The origins of Lake Algonquin's 'Main Phase' have been attributed to the first of several melt-water pulses from the vast pro-glacial Lake Agassiz in what is today southern Manitoba and north-west Ontario into the Great Lakes Basin (GLB) (Kor 1991; Lewis & Anderson 1989). Now dated to *c*. 13,100 and 11,100 cal. BP (years before AD 1950) (Moore *et al*. 2000), the Main Phase had a significant effect on the hydrological evolution of GLB. During this period Algonquin was the most extensive lake in the GLB, covering an area greater than 120,000km^2 and filling the basins of lakes Huron and Michigan, and incorporating the smaller modern lakes Nipissing and Simcoe in north-east and north-central Ontario, respectively, as well as large stretches of adjacent land.

In 1970s, and building on earlier work (e.g., Chapman 1954), Harrison (1972) and Chapman (1975) identified a complex of eastward outlet sills at progressively lower elevations south and southeast of North Bay. All of these outlets drained into the Mattawa-Ottawa valley and took the lake through a series of nine 'post-Algonquin' phases (with associated outlets): Ardtrea (Fenelon Falls), Upper and Lower Orillia (Port Huron?), Wyebridge (South River), Penetang (Genesee), Cedar Point (Fossmill), Payette (Sobie-Guilmette), Sheguiandah (Mink Lake) and Korah (Windigo Lake) (Chapman 1975; Harrison 1972; Heath & Karrow 2007; Karrow 2004; Lewis & Anderson 1989; though see Schaetzl *et al*. 2002 who have proposed a series of four or five phases). Most remain undated radiometrically, but the sequence is thought to have taken hundreds rather than thousands of years to complete (Lewis & Anderson 1989). The first outlet (associated with the Ardtrea phase) started to open *c*. 11,200-11,100 cal. BP (Moore *et al*. 2000); the last (associated with Korah) led to the creation of the Stanley (Lake Huron) and Hough (Georgian Bay) low-stand (*c*. 9500-8400 cal. BP), and appears to have incorporated at least two periods of hydrological closure within the GLB: *c*. 9500-9300 cal. BP and *c*. 9000-8400 cal. BP (Brooks, Medioli & Telka 2010; McCarthy & McAndrews 2010; McCarthy *et al*. 2010). These two latter periods were separated by a large but probably short-lived melt-water pulse from palaeo-Lake Superior *c*. 9300 cal. BP that discharged through the Huron-North Bay-Ottawa river system into the St. Lawrence sea-way. An event thought to have instigated a widespread climatic cooling event in the North Atlantic (Yu *et al*. 2010).

Changes in the drainage outflow from Lake Agassiz – and likely also from the pro-glacial lakes Barlow and Ojibway, which lay to the south and north of the Hudson Bay-GLB watershed divide, respectively – would continue to cause fluctuations in lake levels during the post-Stanley-Hough, Main Mattawa lake phase in the GLB. The Agassiz-Barlow-Ojibway system appears to have coalesced into a single body of water *c*. 8900 cal. BP, ahead of abrupt extinction during the final break-up of the Laurentide in Hudson Bay. Possibly occurring in two stages between *c*. 8470-8205 cal. BP, this break-up has been cited as the probable trigger behind the '8.2 Cold Event' in the North Atlantic (Clarke *et al*. 2004; Haberzettl, St-Onge & Lajeunesse 2010; Lewis *et al*. 2012; *cf*. Rohling & Pälike 2005; Veillette 1994). In Hudson Bay itself, the maritime Tyrrell Sea (Lee 1960) had already started to encircle the decaying ice sheet *c*. 9000-8000 cal. BP. Based on the recovery of low concentrations of marine microfossils in lake sediment, marine waters had probably penetrated Lake Ojibway shortly before its demise (Roy *et al*. 2011). The Tyrrell Sea flooded large swathes of northern and western Quebec. A shift in the depositional character of sediments in north-western Quebec from marine to lacustrine *c*. 6330-6150 cal. BP marks the end of this transgression, though brackish water conditions appear to have persisted until *c*. 3620-3360 cal. BP in some areas (Miousse, Bhiry & Lavoie 2003).

Within the GLB, the Stanley-Hough low-stand ended *c*. 8300 cal. BP, following the demise of Agassiz-Barlow-Ojibway and coinciding with the onset of wetter climate conditions regionally (Lewis *et al*. 2008). Available dates, recalibrated here from older assays, for the subsequent Nipissing phase – 7415-7704 cal. BP (BGS-224) to 5277-5487 cal. BP (BGS-127) (Terasmae 1979) – do not follow directly after the end of the Stanley-Hough low-stand. The water levels of the Nipissing phase did not attain those of the Mattawa, though drainage again passed through the North Bay area until isostatic recovery shifted discharge to southern outlet sills near Chicago and Port Huron (Lewis & Anderson 1989).

It is increasingly apparent that the life-history of these lakes – the fluctuations in water level and drainage that they track through the Early Holocene – was marked by complex and abrupt shifts (e.g., Luz *et al*. 2007; Roy *et al*. 2011; Teller 1995; Wu *et al.* 2010). Despite this, their shorelines appear to have been a focus for human activity during the initial Early Palaeoindian occupation of southern Ontario (e.g., Jackson *et al*. 2000; Storck 1982, 1997, 2004). Complementary archaeological evidence from north-east and north-central Ontario is more limited and later. While it also appears to have been associated with lake margins (e.g., Greenman 1943, 1966; Julig & McAndrews 1993; Phillips 1988, 1993), recent underwater surveys in upper Lake Huron have revealed archaeological features thought to date to the Early Holocene that are interpreted as structures used for hunting caribou (O'Shea & Meadows 2009; O'Shea *et al*. 2014); findings that signify both a terrestrial resource draw into the north and possibly another facet of early occupation. The site of Sheguiandah, on Manitoulin Island, *c*. 10,600 cal. BP (Julig & McAndrews 1993; Lee 1957) is one of the few to have been systematically studied along the shores of Lake Huron and likely marks the earliest possible presence of people in this part of the GLB. Its existence is a further indication that the biological productivity of the landscape was already sufficient to attract groups north (Julig 2002).

Lake sediment cores from sites across northern Ontario continue to be used in palaeoenvironmental reconstruction (*see* e.g., Anderson 2002; Breckenridge *et al*. 2012; Lewis & Anderson 2012; Warner, Hebda & Hann 1984), though further attention to the North Bay area has been limited (e.g., Anderson, Lewis & Mott 2001). In this paper we examine multiple proxies from a new core extracted from a kettle lake northeast of North Bay, near the hamlet of Balsam Creek.

Kettle lakes form where an ice-block has detached from a retreating glacier and become partly buried under outwash deposits. Eventual melting of the ice causes a hollow to form as the ground surface subsides. This change in local topography can then cause meltwater to be diverted into them, creating a small lake within the kettle basin (Bennett & Glasser 2009). The Balsam Creek kettle is located within a large elevated and flat-topped glacio-fluvial outwash delta *c*. 4km long and 2.5km wide (Gartner 1980; *see* Figure 1b). Karrow (2004) hypothesised that sediments within the kettle may yield dating potential for the minimum age of delta formation and hence insights into the drainage chronology of post-Algonquin lake phases in the vicinity of North Bay. For this study we also considered that the location could provide a valuable point of reference within the dynamic Early-Mid Holocene inter-lacustrine deglacial environments that existed between Lake Barlow expanding to the north, and the post-Algonquin lakes to the west and south of the delta (*see* Lewis *et al*. 1994). We saw further potential in the site to provide information on the stability and productivity of kettles within this changing landscape, including in the context of early Palaeoindian activity in northern Ontario.

2. GEOLOGICAL SETTING

The area northeast of North Bay lies geologically within the Central Gneiss Belt (western Grenville province, Tomiko domain). It is characterised by undifferentiated gneisses and migmatites with an age of *c*. 1.16Ga, underlain by Proterozoic (2.5-0.5Ga) metasedimentary gneisses (Ketchum & Davidson 2000). Small occurrences of lower Paleozoic (0.54-0.25Ga) rocks, including limestone, occur under Lake Nipissing to the west (Lumbers 1971). The late Quaternary landscape comprises hilly, rocky, mostly forested terrain mantled with varying thicknesses of glacial drift. Topographic relief varies from 200-400m, with an east to west lowland extending westward along the north shore of Lake Huron to Sault Ste. Marie, adjacent to Lake Superior. Along the northward-rising slope of the lowland is where the northernmost of the Algonquin shorelines are found (Cowan 1985; Heath & Karrow 2007).

Glacial deposits consist of coarse gravelly till, thinly covering bedrock with thicker accumulations in rare, discontinuous terminal moraine ridges. Associated glaciofluvial sands and gravels comprise eskers and outwash deposits; glaciolacustine clays and silts are found in lowland areas. Major glacial features in the landscape local to the Balsam Creek coring location (closed white circle) are shown in a Digital Elevation Model (DEM, vertical accuracy: ± 1m) (Figure 1a), courtesy of data from Ontario Ministry Natural Resources and Forestry (MNRF 2016). The site lies close to a likely esker conduit emanating from the retreating ice-margin and is associated with an unnamed moraine situated between the

Cartier I / Lake McConnell moraine belt and the Rutherglen moraine (Daigneault & Occhietti 2006; Dyke *et al*. 1989; Veillette 1988, 1994). The Cartier I / Lake McConnell moraine belt dates to sometime between 13,083-11,703 cal. BP (Hel-400) and 10,600-10,204 cal. BP (GSC-1851) (Saarnisto 1974), and probably reflects the position of the ice-margin during the Younger Dryas cold interval (12,700-11,700 cal. BP) (Lowell *et al*. 1999; Occhietti 2007).

Abandoned shorelines are also ubiquitous in the area (Figure 1a) and are demonstrated in two transects (T1 and T2) derived from interpolation of the digital elevation data (Figure 1b). Given that the rim of the Balsam Creek kettle has an elevation of *c*. 357m (section 3.1) it would likely have been subject to inflow or inundation when surrounding pro-glacial lake levels lay between the S1 (376m asl) and S4 (362m asl) shorelines of T1, and S2 (371m) and S4 (360m) shorelines of T2 (Figure 1b). This would make the earliest likely period when vegetation could colonise the kettle vicinity and peat begin to accumulate as lying between S4 and S5 (357m asl) of T1 (Figure 1b). The S4 shoreline on T1 is tentatively correlated to the Payette lake phase and water plane elevation in the Balsam Creek vicinity, while S5 likely equates with the Sheguiandah phase (*after* Karrow 2004).

<< **Figure 1a:** A regional-scale Digital Elevation Model (DEM; MNRF 2016) showing glacial and glacial lake features, including a preliminary aggregation of moraine ridges (thick black lines) into contemporaneous ice marginal positions (shaded grey areas). The coring location is marked by a white circle; the extent of Figure 1b is shown in the black rectangle (image: R. Mulligan). Inset map (redrawn from Karrow 2004) shows study area relative to the Great Lakes. >>

<< **Figure 1b:** Annotated DEM (MNRF 2016) showing the glacial features in the area immediately surrounding the coring location (white circle; *see* 1a for legend). Two transects (white lines; T1, T2) derived from digital data are highlighted and projected to the line of maximum uplift (N21°E; Karrow 2004). T1 shows five subtle shorelines (S1-S5), which are correlated to four of the ten shorelines on T2 (S2-S5), based on the magnitude of uplift along the 8.5km separating the two transect areas. Inset map shows the level of detail within the 2x2m (cell size) DEM in the local area. Vertical scale on transects is in metres above sea level (asl), horizontal scale divided into 50m increments (image: R. Mulligan). >>

3. METHODOLOGY

3.1 Field methods

The Balsam Creek kettle is situated *c*. 34km northeast of North Bay on Highway 63 (46°28'57.43"N, 79°09'02.63"W; Ontario Ministry of Natural Resources map 20 17 6400 51400) (Figure 2). Ontario Ministry of Natural Resources-approved survey work of the kettle was carried out in August 2010 and January 2011. The shoreline has an elevation of *c*. 332m asl whilst the rim of the bowl is *c*. 25m above this level. Based on our field observations, indications are that during the spring and early summer a shallow lake currently forms in the bottom of the kettle to a depth of perhaps 0.5m over most of its surface area of just under 1.48 acres (5989m^2) – obtained using the area function on a Garmin Oregon 300 handheld GPS. No input channels or streams were identified, further supporting a seasonally ephemeral nature. Two west-east transects were sampled every 5m using a 3m soil probe. A substantial increase in sediment depth (>3m) was identified towards the central-east side to the kettle – the area where water still pools on the surface. This was in-keeping with expectations about rates of highest sediment accumulation in kettle lakes (Lehman 1975). The location of these deposits was staked and GPS-tagged as 46° 28′ 57.3″N, 079° 09′ 02.9″W for winter coring.

<< **Figure 2**: Looking towards the north-west end of the kettle across the shallow pool that remained on the lake-bed in late summer 2010 and from where cores were later extracted (photograph: R. Rabett). >>

Two paired-cores were extracted within a 5m radius of the tagged location over the course of three visits in January 2011. Each core was extracted using an Eijkelkamp piston auger (38mm bore), through *c*. 20.5cm diameter holes drilled through the lake ice – which had frozen down to the lake bed. The combined recovered sections produced total core lengths of: 204cm (Blue 1), 297.5cm (Blue 2), 262cm (Orange 1) and 363.5cm (Orange 2). A composite core was studied for this report, combining the longest of the Blue series cores and the bottom-most section of the longest Orange series core, extending to the maximum recovered depth of 363.5cm. Note that all depths are given as 'core depth' measurements and are not necessarily an accurate measure of deposit depth.

3.2 **Laboratory methods**

The use of multiple lines of independent proxy evidence has become central to reconstructing early postglacial lacustrine environments and to accurately tracking changing conditions within them (e.g., Daubois *et al.* 2015; Hu *et al*. 1999; Liu 1990; Lutz *et al*. 2007; Teller *et al*. 2008; Wolfe *et al*. 1996; Yu 1994, 2003). Seven lab-based proxies were applied to our analysis of the Balsam Creek record. AMS radiocarbon dating and Bayesian age-depth modelling were used to create a complete chronostratigraphy, with cryptotephra analysis to extend and enhance existing regional ash distribution data and to explore potential feedback mechanisms between vegetation and climate. X-Ray Fluorescence (XRF) was employed in order to determine the relative elemental composition of the lake sediments. Magnetic susceptibility assessed changes in sediment character that can be related to palaeoenvironmental and climatic variation. Loss on ignition (LOI) was used to examine changes in the organic and carbonate content of the sediment column. Palynology was employed to identify vegetation taxa and succession dynamics. Bulk organic $\delta^{13}C$ isotopic analysis tracked changes in prevailing vegetation type and photosynthetic responses to climate change.

3.2.1 Chronostratigraphy

All AMS ^{14}C dates used to establish the chronostratigraphy of the Balsam Creek core and, unless otherwise stated, all other dates mentioned in the text were calibrated against the IntCal13 curve (Reimer *et al*. 2013) and use the Calib Radiocarbon Calibration Programme (Calib. Rev. 7.0.0) (Stuiver & Reimer 1993). In order to clarify understanding about changes in sedimentation at this location through time, and to refine our observations particularly where these related to the basal oscillations, we employed an age-depth modelling technique (*Bacon*) that utilises the open-source statistical environment R to create Bayesian age-depth models (Blaauw & Christen 2011). *Bacon* calibrates ^{14}C dates against a specified curve (in this case, IntCal13) and can incorporate known calendar age markers, such as tephras, into its age-depth projections. Our model (Figure 3) utilised default settings: i.e. piece-wise linear model with 5cm sections, a gamma prior for sedimentation times with mean 20 and shape 1.5, a beta prior for memory with mean 0.7 and strength 4, and a student-t distribution to deal with outlying dates. All modelled dates presented in this report are rounded to the nearest 5yrs; unrounded values are presented in Supplementary Table 1.

For the cryptotephra analysis, contiguous 5cm stratigraphic intervals were sub-sampled as rangefinders to provide an initial overview of glass shard concentration throughout the core and to locate intervals with possible cryptotephra layers. Rangefinder samples were ashed for 2 hours at 550 °C to remove organic material, followed by sieving between 80 and 25μm to remove coarse particles >80μm and obscuring silts and clays <25μm. The >25μm fraction was then subjected to the centrifuge floatation method of Blockley *et al*. (2005) to float out lower density volcanic glass shards from the relatively heavier host mineral matrix. Floated residues, including any shards present, were then mounted onto glass slides (glycerol media) and shard concentrations counted using a high-power Olympus CX40 light microscope at ×100 and ×400 magnifications. Those 5cm rangefinders with the highest shard concentrations were further sub-sampled at 1cm contiguous intervals (1cm^3) and prepared and analysed in the same manner. This enabled us to determine the stratigraphic depth to 1cm accuracy of maximum shard concentrations within the core. Shards were picked from the concentration peaks, mounted in resin and sectioned and polished for geochemical characterisation by electron probe microanalysis with wavelength dispersive spectroscopy (WDS-EPMA) at Queen's University Belfast and the Tephra Analysis Unit, University of Edinburgh. Rhyolitic Lipari secondary standard was used to test analytical consistency in both probes. All EPMA geochemical data were normalised to 100% on a volatile-free basis for correlation purposes between layers and reference data used in biplots and similarity coefficient calculations. The similarity coefficient score is a simple measure of multivariate similarity between the major oxide elements present (Borchardt, Aruscavage & Millard 1972). (Supplementary Table 2 contains original un-normalised EPMA data).

3.2.2 X-Ray Florescence (XRF)

The X-ray fluorescence (XRF) scanning of sediment cores allows for non-destructive, relatively high resolution mapping of changes in relative elemental composition. Core surfaces were prepared by scraping with a stainless steel scraper to produce a clean, flat surface. The core surface was then covered with 4μm thin SPEX Certiprep ultralene film, which is relatively translucent to X-rays. Measurements were made on a 3rd generation Avaatech scanner at the Godwin Laboratory, University of Cambridge. Measurements were made at 2.5mm intervals at 10kV (no filter, 0.75μA), 30kV (thin Pb filter, 0.5μA) and 50kV (Cu filter, 1.0μA) with 40 second count times for each measurement. The scanning window was 2.5mm down-core and 12mm cross-core. Principal Component Analysis (PCA) was then applied to the resulting data. PCA is a well-documented technique for identifying the major components of shared variance in complex datasets, 'distilling' multiple records to generate a few factors that describe the major sources of variance shared between those records. In the case of the Balsam Creek data, the logs of the XRF count ratios to Al of Cl, Si, Ca, Ti, Mn, Fe, Rb, Sr and Zr were analysed, following Weltje and Tjallingi (2008).

3.2.3 Magnetic Susceptibility and Loss on Ignition

The magnetic susceptibility profile was measured at 2cm intervals using a Bartington MS2C magnetic susceptibility meter with 100mm diameter (Thompson et al. 1980). Sediment samples of 1cm3 were then collected at 2cm intervals for loss on ignition (LOI) analysis. Following the LOI protocol used at the Physical Geography Laboratories at the University of

Cambridge, LOI samples were heated sequentially for periods of at least 6 hours at 105, 400, 480 and 950°C and the results used to calculate %water, %organic matter, %elemental carbon (charcoal), %$CaCO_3$ and %mineral residue respectively. These thresholds ensure separation between the constituent components while minimising or completely removing any interference caused by loss of structural water from clays that occurs above 500°C (Heiri *et al*. 2001; Keeling 1962; Ball 1964).

3.2.4 *Palynology*

Samples were analysed at 4cm intervals for pollen. Laboratory procedures and sample preparation techniques followed those outlined by Faegri and Iversen (1989). Analysis of the prepared slides was conducted on a high-power Olympus BX41 light microscope using ×40 and ×100 magnification. Tilia and TGView (Grimm 2004) were used for data processing and diagrammatic representation, respectively. Pollen percentages were calculated on the basis of the total terrestrial pollen sum. Zonation of the pollen diagram was performed employing CONISS, using taxa recorded at ≥ 5% as the statistical parameter. On the diagrams minor species have had an exaggeration (×5) curve applied. The principal pollen reference material used in this study was McAndrews *et al*. (1973).

3.2.5 *Bulk organic $\delta^{13}C$*

Plant $\delta^{13}C$ is primarily determined during photosynthesis and is affected by any factor influencing this process (O'Leary 1988). Samples collected for bulk isotopic analysis were collected at 8cm intervals and leached in 0.1M HCl for 48hrs to remove sedimentary carbonates (already known to comprise only a small percentage by weight of the sample based on LOI analysis). Samples were then washed in distilled water and dried in a convection heater at 40-80°C. The remaining organic-rich sediments were crushed with pestle and mortar, and 0.8-1mg of sample by weight was placed into tin capsules. These prepared samples were isotopically analysed in triplicate using a Costech elemental analyser coupled in continuous flow mode to a Finnigan MAT253 mass spectrometer, located in the Godwin Laboratory, Department of Earth Sciences, University of Cambridge. Results are reported as mean values in parts per thousand (‰) relative to the Vienna Pee Dee belemnite (V-PDB) international standard. Measurement errors were less than 0.2‰.

4. RESULTS

4.1 Sedimentology

Throughout its length the cored profile preserved an abundance of waterlogged macro-remains including large woody fragments, smaller woody pieces, reeds and root matter in various stages of decay. Visual inspection of the individual core sections revealed six major stratigraphic units based on changes in colour, compaction and the size and degree of degradation of organic inclusions, primarily woody remains and reeds (*see* Table 1).

<< **Table 1:** Balsam Creek core, sedimentary unit (U) descriptions. >>

4.2 Chronostratigraphy

Ten AMS ^{14}C dates were obtained on organic matter (wood fragments, seeds, grass and other terrestrial plant macros) taken from across the length of the core (Table 2). These dates attest that the depositional sequence recovered from the Balsam Creek kettle lake tracks vegetation succession from soon after local deglaciation. In this part of Ontario, other studies have indicated that peat accumulation began 10,800-10,500 cal. BP (e.g. Anderson, Lewis & Mott 2001; Terasmae & Hughes 1960).

<< **Table 2:** ^{14}C dates obtained for the Balsam Creek core. All dates were processed through the AMS facility of the ^{14}Chrono Centre, Queen's University Belfast. >>

4.2.1 Age-depth modelling

All of the Balsam Creek AMS dates as well as representative dates for the Mount Mazama and Llao Rock eruptions were inputted into an age-depth model using *Bacon* (*see* Blaauw & Christen 2011). All dates in the series were incorporated in the uncertainty envelope of the model except for UBA-22774 and UBA-25526, which the model bypassed. It is notable, however, that the modelled mean value does not pass through either the estimated age of Llao Rock (*see* Section 4.2.2) or UBA-25525 (345cm). Were we to reduce chronological uncertainty simply to the modelled mean, both of these dates would also have appeared as outliers, suggesting that unidentified (and almost certainly independent) mechanisms are acting on both. From the radiocarbon dates at the bottom of the core until approximately the Mazama tephra layer, sedimentation appears to have been quite slow at *c*. 1cm/100 yr. From then on, the modelled accumulation is much faster and quite constant at *c*. 20 yr/cm.

<< **Figure 3:** Balsam Creek age-depth curve, including independent dates for the Mt Mazama (Egan, Staff & Blackford 2015) and Llao Rock (Foit & Mehringer 2016) eruptions. The dashed black lines indicate depths where cryptotephra was identified within the Balsam Creek profile (284cm & 325cm) (histogram: M. Blaauw). >>

4.2.2 Tephrostratigraphy

At 5cm rangefinder resolution much of the stratigraphy within the Balsam Creek (BCK) core profile contained low shard concentrations (1-2 shards per rangefinder); this can be attributed to background deposition. In four intervals, measuring from the top of the core (12-16cm, 27- 31cm, 283-287cm & 323-328cm) the concentrations exceeded background levels and were further examined at 1cm resolution (Figure 4). Study of these intervals revealed particularly prominent shard peaks at two points: 284-285cm (sample BCK-284; 220 shards cm^{-3}) and 325-326cm (sample BCK-325; 820 shards cm^{-3}). The two remaining upper rangefinder intervals could not be resolved further at 1cm resolution.

Microprobe analysis, using equipment at Belfast and Edinburgh (Supplementary Table 2), revealed that the geochemical composition of both of the lower peaks is calc-alkaline rhyolite. The BCK-284 layer correlates well with the Mazama ash (Figure 5) with a similarity coefficient (SC) of 0.98. This ash from the Mount Mazama climactic eruption (now Crater Lake caldera, Cascade Range, Oregon) deposited visible beds over much of western North America (Bacon & Lanphere 2006), extending predominantly to the northeast, with cryptotephra being deposited as far as Lake Superior (Spano *et al*. 2017) and Newfoundland (Pyne-O'Donnell *et al*. 2012). Distal Mazama ash detected in the Greenland (GISP2) ice-core stratigraphy indicates an age of 7627±150 cal. BP (Zdanowicz *et al*. 1999). A recent compilation of radiocarbon dates by Egan, Staff & Blackford (2015) has employed Bayesian statistical modelling to provide a refined age of 7682-7584 cal. BP. Our modelled age range for 284cm is 7660-7430 cal. BP (mean age: 7580 cal. BP), aligning it closely to the Egan, Staff & Blackford (2015) refined age.

The BCK-325 layer is superficially similar to Mazama ash reference samples (SC: 0.95) (Figure 5). The potential for density-induced settling of tephra shards has been explored in a number of studies (e.g., Anderson, Nuhfer & Dean 1984; Beierle & Bond 2002; Enache & Cumming 2006). These conclude that downward movement can cease at or just beneath a stratigraphic boundary with more dense, less organic sediment, at a point when the density of the sediment is sufficient to support the tephra (Beierle & Bond 2002). Within the Balsam Creek profile, the lower accumulation of Mazama-like ash occurs at a depth that is broadly commensurate with a change in sedimentary unit (Units 6-5). Four lines of evidence, however, allow us to reject a settling hypothesis in this instance. 1) While similar to the BCK-284 ash (*cf*. Beierle & Bond 2002: 436), the tephra retrieved from the BCK-325 layer contains a slightly higher average SiO_2 content (*c*. 1.3 normalised wt%), consistent with it representing a discrete event. 2) There is a clear separation of *c*. 40cm between the two events with no intervening tephra. 3) The BCK-325 tephra was identified within 10mm of the base of the uppermost 125mm band of laminated clay sediments (i.e., 314-326.5cm) in Unit 6. In other words: it was sealed within, not lying on or just within the laminar clays of this unit. 4) Intervals of reduced growing conditions within the kettle observed in the $\delta^{13}C$ data parallel both the BCK-284 Mazama ash layer and the BCK-325 layer. These are the only two such dramatic downturns observed in the profile, suggesting association with separate ash-fall events.

A precursor Llao Rock eruption has been described from rhyodacite lava flows and related pyroclastic deposits in the Crater Lake locality (Bacon & Lanphere 2006). This is believed to have preceded the climactic eruption by *c*. 200 years, with a date of 7015±45 14C yrs BP (7945-7739 cal. BP) from the Crater Lake vicinity (Bacon 1983). A layer of ash identified below Mazama from lakes in south eastern Oregon has also been assigned to Llao Rock, with a mean interpolated age of 6940±100 ^{14}C yrs BP (7953-7609 cal. BP) (Foit & Mehringer 2016).

The close convergence between the published age of Mazama and the modelled age of cryptotephra at BCK-284 is not repeated when we consider the age of Llao Rock against the modelled age of BCK-325, even though there is apparent correspondence between the position of Llao Rock within the age-depth model and the relevant layer in the core (Figure 3). Our modelled age range at 325cm (8710-7865 cal. BP) is considerably older than the range assigned to Llao Rock (7953-7609 cal. BP). The published geochemistry of the Llao Rock eruption presented by Foit & Mehringer (2016) also shows general equivalence to the Mazama ash (SCs: 0.97-0.98). The BCK-325 cryptotephra does not follow this equivalency. Acute decline in the ratio values of Ti/Al, Fe/Al, Rb/Al, Sr/Al and Zr/Al at 316cm and 322cm points to the influx of aluminosilicate minerogenic components from regionally occurring metamorphic geological sources. It is probable that the similarity of the 325cm layer to known Mount Mazama products reflects a southern Cascades source locality (S Kuehn *pers. comm*. to S Pyne-O'Donnell). As yet, though, we cannot confidently assign BCK-325 to Llao Rock for the aforementioned reasons. Until there is further clarification of this relationship, we designate BCK-325 peak as the 'Balsam Creek' tephra.

<< **Figure 4:** Tephrostratigraphy of Balsam Creek showing cryptotephra glass shard concentrations per 5cm rangefinder (grey) and cm^{-3} (red). The cryptotephra layer at 284-285cm (BCK-284) correlates to the Mazama ash, while the 325-326cm (BCK-325) cryptotephra is designated as an uncorrelated Mazama-like layer (data & presentation: S. Pyne-O'Donnell). >>

<< **Figure 5:** Element oxide biplots (wt%) for glass from cryptotephra layers BCK-284 and BCK-325 at Balsam Creek. In each case SiO2 is compared against **A:** TiO_2, **B:** Al_2O_3, **C:** FeO, **D:** MgO, **E:** CaO, **F:** K_2O. The Mazama ash reference (UA 1573) from Edmonton River Valley (Pyne-O'Donnell *et al*. 2012) is shown for correlation. Error bars shown are 2σ of the Lipari standard for the Belfast (red) and Edinburgh (green) microprobes. Note: All data points have been normalised for data set comparison. Supplementary Table 2 contains original un-normalised geochemical source data (data and presentation: S. Pyne-O'Donnell). >>

4.3 X-Ray Fluorescence

Seven chemozones (CZ) were identified in the core by visual inspection of the XRF data (Figure 6, Table 3). The term 'chemozone' is applied semi-quantitatively: as a significantly distinct interval characterised by consistent changes in chemical composition, though such changes are not absolute determinations – i.e., the divisions are 'XRF chemozones'. CZ3 was subdivided to account for significant changes observed in one or more ratio datasets, where the changes were nested within broader trends. Elements Ca, Si, Ti, Fe, Rb, Sr, Zr and Cl were normalised against Al, and expressed as log ratios to help account for non-linearity between element concentrations and intensities (Shackley 2011; Löwermark *et al*. 2011). Lithogenic elements Fe, Rb and Zr were used as proxies for detrital input and Ca/Al ratios were used to measure authigenic contribution. Ca/Sr ratios were used as a hydrology proxy (Cohen 2003) and Si/Al, Ti/Al and Zr/Al were used as proxies for grain size (Aniceto *et al*. 2014). Apparent linear offsets in the XRF counts for all elements in the section from 260 to 295cm, which were attributed to a deconvolution error in the XRF measurements, were corrected prior to PCA using measurements on adjacent depths; Cl measurements were corrected to the base of the studied sequence at 357.75cm. The PCA identified two sources of variance with Eigenvalues greater than one. The first of these components (PC1, *see* Figure 7) accounted for 53.7% of the variance, and has large positive loadings for Ti, Rb, Sr, Zr and Si. It is an indicator of terrigenous sedimentation, particularly in the silt size fraction (Croudace & Rothwell 2015: 72) and this component probably corresponds to generalised terrigenous mineralogical input to the site. High PC1 values may reflect the input of lithogenic materials into the kettle basin. Reduced PC1 values at *c*. 275-290cm and 320-335cm depth broadly correlate with peaks in $\delta^{13}C$ and likely indicate changes in the relative proportions of organic sedimentation versus inorganic carbonate sedimentation.

<< **Figure 6:** Chemozones 1-7 obtained from XRF analysis of the sediment profile. Element data is provided in counts per second (cps). The relationship between chemozones, pollen zones (BC) and sedimentary units (U) is presented against profile depth (data and presentation: L. Farr & S. Crowhurst). >>

<< **Table 3:** Descriptions of discrete chemozones (CZ) within the Balsam Creek core. >>

4.4 Magnetic susceptibility

The core sediments were found to be mostly weakly diamagnetic and showed only minor fluctuations throughout the sequence. This reflects the dominance of organic detritus and non-ferrous minerals (e.g., quartz or calcite) throughout the core. An overall trend, however, toward more negative values was noted towards the base of the Blue 2 core (bottoming at 297.5cm) – magnetic susceptibility was not tested on the basal section of the Orange 2 core. The oscillations throughout the studied sequence (Figure 7) may correlate to minor changes in the proportions of aeolian and/or fluvial sediments to the Balsam Creek kettle sequence, or to changing source-areas for these inputs. The signal may also have been influenced by any magnetotactic bacteria that lived in the lake, but a maximal range of 12 SI units is small and reinforces the overall stability of the lake system. Two point-samples show weakly positive values and may correspond to increased ferromagnetic or paramagnetic inclusions at these depths (54cm & 223cm). Three broad zones are visible in the magnetic susceptibility profile: above 154cm average of –2.1 SI units; 154cm-250cm average of –3.74 SI units; and 250-300cm approx. –5.56 SI units.

4.5 Loss-on-ignition

The loss on ignition data revealed variability in the organic component of the core between approximately 40-70%, being inversely correlated with the mineral residue component which fluctuated between 25-60% (Figure 7). Periods of increased mineral content and/or reduced organics occur particularly at 50-110cm, 165-200cm and in the deepest part of the core below *c*. 320cm. These periods may reflect enhanced input of fine sediments to the lake either by in-washing from local streams or through aeolian deposition. An additional carbonate component varied mostly between 0-10%, again representing inputs from sedimentary sources. Small quantities of 0-4% elemental carbon lost following the 480°C burn were present throughout the upper 250cm of the sequence, indicative of the effects of natural forest fires in the vicinity of the lake. Curiously, this carbon content all but disappeared below 276cm, suggesting that fire was not a significant agent in the local environment during the early post-glacial. As this lower part of the core also produced some of the lowest organic content measurements in the entire sequence (i.e. between 30-50%), it is possible to infer low-density vegetation at this time that was not susceptible to wild fires, or conditions that otherwise reduced the likelihood of their occurrence.

<< **Figure 7:** Compares data for magnetic susceptibility (including mean SI (μ) values), loss on ignition (% water then % dry weight), $\delta^{13}C$, cryptotephra shards and XRF PC1 values (20-357.75cm) from the Balsam Creek core. Pollen zones (BC) and sedimentary units (U) are provided for comparison (data: A. Pryor, L. Farr, S. Crowhurst, S. Pyne-O'Donnell, presentation: R. Rabett). >>

4.6 Palynology

The pollen record at Balsam Creek (BC) was divided into ten depositional zones, starting from the base of the core (Figure 8). Superimposition of these zones onto the sedimentary units was only possible at a broad scale. The two basal zones correspond approximately to sedimentary Unit 6; Zones 3-8 fall within Unit 5; Zones 8 and 9 cover Unit 4; and Zone 10 incorporates Units 3-1. Age estimates for pollen zones are drawn from the core's age-depth model mean values per cm.

<< **Figure 8:** Tilia graph showing the pollen spectra from the Balsam Creek core, sedimentary units and age-depth modelled chronology (data and presentation: D. Simpson). >>

*4.6.1 BC1: 360–342cm (*c. *10,425-8965 cal. BP)*

This zone is characterised by high percentages (*c*. 95-97%) of arboreal pollen. *Pinus* undiff. pollen is abundant throughout (*c*. 51-62%) and is the dominant feature of the zone. *Pinus strobus* values (*c*. 3-6%) are relatively consistent throughout. *Picea* representation rises sharply to maximum representation for the sequence at the beginning of the zone with values remaining relatively high thereafter. *Betula* (*c*. 6-16%) and *Quercus* (*c*. 4-7%) are the main deciduous elements with fluctuating values for both taxa throughout the zone. *Betula* values (16%) rise sharply at the termination of the zone. *Abies* (*c*. 0-3%), *Carpinus/Ostrya* (*c*. 1-3%), *Myrica* (*c*. 0-1%) and *Ulmus* (*c*. 1-2%) are also represented throughout. Herbaceous taxa (*c*. 1-5%) representation in this zone is the highest of the sequence. *Ambrosia* (*c*. 0-2%) and Cyperaceae (*c*. 0-2%) are the two main species represented. Values for both types decrease consistently as the zone proceeds towards termination.

4.6.2 BC2 : 342–326cm (c. 8965-8200 cal. BP)

Arboreal pollen (*c*. 92-95%) dominates this zonal assemblage, with *Pinus* undiff. the dominant component (*c*. 53-62%). Values for both *Pinus* undiff. and *Pinus strobus* (*c*. 5-9%) display a generally increasing trend as the zone proceeds. *Betula* (*c*. 8-13%) is relatively constant throughout the zone, although overall there is a decreasing trend as the zone progresses. Values for *Picea* (*c*. 2-6%) reflect a similar trend in this zone with values reduced to 2% at the termination. There is a noticeable spike in values for *Alnus* (2.5%) at the transition with the zone BC3; *Quercus* (*c*. 4-6%) is again constantly present. *Abies* (*c*. 1-2%), *Alnus* (*c*. 0-3%), *Carpinus/Ostr*ya (*c*. 2-3%) and *Ulmus* (*c*. 1-2%) are the other main arboreal taxa represented. With the exception of *Carpinus/Ostrya,* the representation of these species increases as the zone progresses. Representation of herbaceous taxa is low (*c*. 2-4%). A marked increase in values for *Lycopodiaceae* undiff. (*c*. 2-3%) was noted in this zone.

4.6.3 BC3: 326-298cm (c. 8200-7800 cal. BP)

BC3 is characterised by high values of arboreal pollen (*c*. 91-97%) present in relatively stable abundances throughout. Values for both *Pinus* undiff. (*c*. 52-69%) and *Pinus strobus* (*c*. 4–7%) decrease as the zone progresses. Conversely, *Betula* values increase throughout the zone, rising markedly from 3.9% to 16.9% by its termination. Other consistent arboreal features are *Abies* (*c*. 1-2%), *Alnus* (*c*. 0-2%), *Larix* (*c*. 0–2%), *Picea* (*c*. 0-3%), *Quercus* (*c*. 2-5%), *Tsuga* (*c*. 1-5%) and *Ulmus* (*c*. 1-3%). Of these the values for *Picea*, *Ulmus* and in particular *Tsuga* all increase as *Pinus* values decrease. *Ambrosia* (*c*. 0-2%), Cyperaceae (*c*. 0-1%) and Poaceae (*c*. 0-2%) are the main herbaceous elements. The values for the aquatic *Nuphar* (*c*. 0-3%) increase steadily throughout whereas *Lycopodiaceae* undiff. values (*c*. 0-1%) decrease throughout.

4.6.4 BC4: 298–274cm (c. 7800–7200 cal. BP)

Significant decreases in the overall values for *Pinus* undiff. (*c*. 40-57%) are notable in this zone. An opposing trend is apparent in the values for *Pinus strobus* (*c*. 17-34%), which are in general significantly increased in this zone. A peak in *Picea* (6.3%) at the start of the zone is short-lived and values (*c*. 1-6%) decline sharply thereafter. *Betula* values (*c*. 7-16%) also decrease as the zone continues but do recover slightly at the termination of the zone. *Quercus* (*c*. 2-7%) is, with one exception mid-zone, consistently represented throughout. *Ulmus* (*c*. 1-3%) representation is slightly increased in this zone. *Ambrosia* and *Artemisia* are the main herbaceous elements represented. *Nuphar* values (*c*. 0-1%) are markedly decreased from the previous zone. *Lycopodiaceae* undiff. values (*c*. 2-3%) recover at the start of the zone but drop away sharply as the zone progresses.

4.6.5 BC5: 274-226cm (c. 7200–6020 cal. BP)

Pinus undiff. (*c*. 43-59%) is re-established as the dominant feature of this zone, although values do drop off sharply as the zone concludes. *Pinus strobus* representation (*c*. 14-29%), which is generally lower than in the BC4 fluctuates throughout the zone. This fluctuation is negatively correlated in the values for *Betula* (5-14%), which are displaying an increasing trend as the zone progresses. *Quercus* (*c*. 2-5%) is again a relatively stable constant feature throughout the zone. Noticeable peaks in both *Ulmus* (*c*. 1-4%) and *Corylus avellana* (*c*. 0-2%) are apparent in the upper half of the zone before dropping away at the BC5-6 junction. Poaceae representation follows a similar pattern. An opposing trend is apparent in the representation of *Pteridophyta* (monolete), which peaks at the start of the zone. Both *Carpinus/Ostrya* and *Fagus* values are indicative of decreasing representation as the zone continues.

4.6.6 BC6: 226-176cm (c. *6020–4795 cal. BP)*

While remaining relatively high *Pinus* undiff. values (*c*. 42-68%) indicate significant fluctuation in the representation of the species during this period, with an overall decreasing trend apparent from the middle of the zone onwards. The fluctuation in *Pinus* undiff. representation is also negatively reflected in the representation of *Betula*. Overall *Betula* values (*c*. 7-29%) are higher than those previously recorded and indicate a general increase in representation as the zone progresses. In contrast, *Pinus strobus* is becoming less of a characterising feature, with values (*c*. 8-15%) significantly lower than those recorded in the 2 previous zones (BC4 & BC5). *Tsuga* attains maximum sequence representation (6%) in the lower half of this zone (215cm, mean age: 5761 cal. BP), before declining and then stabilising at 1-2% by 195cm (mean age: 5275 cal. BP). Peaks in *Alnus* at the mid-point of the zone and *Picea*, *Carpinus/Ostrya* and *Nuphar* at the termination of the zone are of note. Similar termination peaks are also reflected in the representation of Cyperaceae, *Isoetes* and Lycopodiaceae undiff. Poaceae continues to be consistently represented after the peak in BC5.

4.6.7 BC7: 176–152cm (c. *4795-4185 cal. BP)*

Consistent presence of both *Nuphar* and *Isoetes* throughout this zone indicates increased representation of aquatic pollen types in the record. Values for *Pinus strobus* (*c*. 14-23%) recover slightly, while the representation of *Pinus* undiff. (*c*. 43-55%) continues to follow the decreasing trend apparent from the mid-point of BC6. *Betula* values (*c*. 17-22%) remain at the higher levels recorded in the previous zone. *Abies* values (*c*. 0-2%) recover after being all but absent in the previous two zones.

4.6.8 BC8: 152-116cm (c. *4185–3285 cal. BP)*

Pinus undiff. values (*c*. 49-60%) recover slightly at the commencement of this zone but have a generally decreasing trend as the zone continues. Values for *Pinus strobus* (*c*. 6-13%) decline to similar levels to those recorded in BC6. The increasing trend in *Betula* representation (*c*. 17-24%) continues. *Myrica* values (*c*. 0-2%) indicate a slight increase and more constant presence of the species. Representation of the other arboreal types in the record i.e., *Quercus*, *Ulmus* and *Corylus avellana* are relatively stable and show very little variability when compared to the values recorded in the previous zones. Consistently higher representation of *Nuphar* pollen (*c*. 1-3%) and to a lesser degree, *Isoetes* (*c*. 0-2%) increase the overall representation of aquatic types (*c*. 1-5%) in this zone. It is of note that while not identified or counted, the frequency of diatoms present in the samples increased from this point in the record onwards, with some samples in the succeeding zones reflecting very significant increases in diatom accumulations.

*4.6.9 BC9: 116–68cm (*c. *3285–2225 cal. BP)*

Betula values (*c.* 21-31%) continue to increase steadily with very little fluctuation in intra zone representation. Values for both *Pinus* undiff. (*c.* 42-53%) and *Pinus strobus* (*c.* 8-16%) continue to decrease slightly, although values are less consistent as the zone progresses and fluctuate to a greater degree within the zone. *Abies* (*c.* 0-2%) and *Picea* (*c.* 0-2%) are more consistent elements in this zone. Representation of the other main arboreal elements remains relatively stable. However, *Quercus* values (*c.* 2-5%) indicate a slight increase in representation. Cyperaceae (*c.* 0-1%), *Nuphar* (*c.* 1-3%) and *Isoetes* (*c.* 0-2%) continue to be consistently represented in this zone.

*4.6.10 BC10: 68–30cm (*c. *2225-1050 cal. BP)*

After a peak in *Betula* values (37%) at the beginning of this zone the overall values return to the levels represented in the previous zone (*c.* 21-30%). *Pinus* undiff. values (*c.* 36-54%) represent a continued indication of the generally decreasing trend apparent in the previous zones (BC8-9). After a sharp decline at the beginning of the zone *Pinus strobus* values (*c.* 7-15%) rise quickly and the decreasing trend apparent in the previous zone appears to stabilise as the zone proceeds. *Alnus* representation (*c.* 0-1%) is slightly decreased. *Abies* (*c.* 1-4%) and *Picea* (*c.* 0-3%) representation continues to increase in this final zone of the record. The values for *Carpinus/Ostrya* (*c.* 0-2%), *Corylus avellana* (*c.* 0-3%) and *Salix* (*c.* 0-1%) are all increased in this zone. Representation of the other arboreal components remains relatively analogous with that of the previous zone. Increased presence of *Ambrosia* (0-1.3%) elevates the overall values for the upland herbs (*c.* 1-4%) particularly towards the termination of the zone. Cyperaceae (*c.* 0-2%) and *Nuphar* (*c.* 1-4%) continue to be consistently represented at levels similar to those in the previous zones.

4.7 Bulk organic $\delta^{13}C$

The bulk organic $\delta^{13}C$ data from Balsam Creek (Figure 7) produced a C_3-dominated signal through-out the core sequence, as one would expect for a higher latitude (i.e., 45-50 degrees) Holocene environment (e.g., Sage *et al.* 1999; Schiff *et al.* 1997). The mean bulk organic $\delta^{13}C$ signal divides approximately into three. It was stable at *c.* –27‰ for the upper 154cm of core, with a maximum increase to –26.3‰ at 58cm towards the base of sedimentary Unit 2. Between 154cm and 270cm, corresponding with pollen zones BC7 to BC5, the mean $\delta^{13}C$ was slightly enriched: falling mostly between –25 and –26‰. By contrast, the lower part of the core (pollen zones BC1 to BC4) exhibited two large increases in $\delta^{13}C$ that align exactly with the presence of the ash-fall discussed above. This profile reflects substantial changes in the terrestrial and potentially aquatic carbon cycle during the sampled period, with points of transition at *c.* 7096 cal. BP (mean modelled age at 270cm) and again at *c.* 4237 cal. BP (154cm). These three broad zones identified in the bulk $\delta^{13}C$ are reflected in the magnetic susceptibility profile, where above 154cm there is a mean value of –2.1 SI units, 154-250cm a mean of –3.74 SI units, and 250-300cm a mean of –5.56 SI units), supporting the interpretation of vegetation and sedimentary dynamics at these intervals.

5. DISCUSSION

5.1 Early Holocene – Vegetation zones (BC1 to BC5)

Sedimentary profiles obtained in the immediate vicinity of North Bay form points of comparison to this study. These include one profile from the vicinity of the Fossmill outlet, though this proved to be too young to record the opening of the outlet itself, with a basal age of 7175-6739 cal. BP (GRO-1924) (Terasmae & Hughes 1960). Two other profiles have been taken north of the city as part of unpublished academic theses (those of H. Ignatius and K.B. Liu) (Ritchie 1987; Terasmae & Hughes 1960). These indicated that peat accumulation had begun *c*. 10,800 cal. BP within a landscape that was marked by short-lived peaks in mixed conifer-hardwood forest species; taxa that would become more dominant here after *c*. 8,900 cal. BP. A third study (Anderson, Lewis & Mott 2001) re-cored Turtle Lake ('Boulter' township lake), which had been previously cored and controversially dated by Harrison (1972). Their new AMS radiocarbon date, obtained on a terrestrial seed, suggested the area was deglaciated and peat had begun to accumulate by 10,795-10,557 cal. BP (CAMS-46195). This was later than Harrison had proposed, but agreed with other local estimates, with the southern Ontario evidence (Karrow *et al*. 1975; Mulligan, Elyes & Bajc 2018; Terasmae & Hughes 1960), and is in close agreement with the age-depth model of this study, which gives a range of 10,670-10,320 cal. BP (mean age: 10,480 cal. BP) at the base of the core (363cm) (Supplementary Table 1).

The basal dates from Balsam Creek provide a minimum age range for the formation of the outwash delta within which the site is situated. However, the buried ice that gave rise to the kettle may have taken time to melt following glacial retreat and local pro-glacial lake drainage. As a result, there is likely to be a time-lag between these events, the development of the kettle and onset of peat accumulation. Nonetheless, the age of the earliest deposits here make it less likely that the nearby Cartier I / Lake McConnell moraine belt dates to the younger limit (10,600-10,204 cal. BP) proposed by Saarnisto (1974), and more likely that it marks the ice-margin as it stood during the late Younger Dryas – in-keeping with other later studies (e.g., Lowell *et al*. 1999; Occhietti 2007).

Shoreline elevation data (Karrow 2004) suggests that the last time this vicinity was under water (and before the kettle formed) was likely to have been during the Payette lake phase, to which we can now also ascribe the minimum age of >10,480 cal. BP. While fluctuations appear to have occurred in the size of the kettle lake post-Payette, there are no indications that it was inundated subsequently.

The plant species represented at the base of the sequence (BC1) suggest that a relatively well-established mixed woodland community with open habitat elements was already in existence. The conifers *Pinus* undiff. and *Picea* dominate the local forest, with *Betula*, *Quercus* and *Carpinus*/*Ostrya* being the main hardwood elements present. With a mix of both shade-tolerant (*Carpinus*/*Ostrya*) and shade-intolerant (*Betula*) species represented, it is difficult to surmise confidently as to how open or closed the forest environment was at this time. Our isotopic data (Figure 7) does not show obvious or significant impact from a canopy effect, which can lower the $\delta^{13}C$ of an ecosystem by 3-5‰ (Drucker & Bocherens 2009; Bonafini *et al*. 2013). Other studies have identified a tundra or forest/tundra phase immediately after deglaciation (e.g., McAndrews 1997; Mott & Farley-Gill 1978, 1981). The presence of the open indicator taxa, such as *Ambrosia*, Asteraceae and Poaceae, suggests that such a phase is probably represented at Balsam Creek, though consequently this disagrees with the observations of Fuller (1997) who proposed that, due to a lag between deglaciation and the melting of the buried ice which formed kettle lakes, the tundra phase may have passed before sedimentation commenced. Three bulk organic $\delta^{13}C$ measurements for BC1 have a mean value of –27.2‰, similar to the top 1.5m of the core and are consistent with the wet and stable growing conditions indicated by the pollen data.

Within BC2, leading up to the first of the intervals recorded in the $\delta^{13}C$ deviations (which continues into BC3) the recorded occurrence of *Picea* drops significantly. It appears to recover at a lower frequency, before dropping again after the second $\delta^{13}C$ interval (within BC4). By the termination of BC4 (*c*. 7200 cal. BP) this taxon becomes a very minor woodland component. The *Picea* record for Balsam Creek fits well with the regional record for *Picea*, which has been recorded at multiple sites across southern Ontario (Fuller 1997). In these other records this genus dominates in the landscape for *c*. 1000 years, after which it declines to low levels as it is replaced by successional species such as *Pinus* and *Betula*. Other elements of the immediate woodland though remained comparatively unchanged, with *Pinus* undiff. continuing to be the major element within the community.

The increase in *Betula* at the BC1-BC2 transition (*c*. 342cm, 8965 cal. BP) suggests more open environments, which may also be reflected by the increase in bulk organic $\delta^{13}C$ to –26‰ at this time. *Nuphar* implies that the water in the kettle was open and shallow during this period. The Cyperaceae in the record would also imply that the local environs surrounding the lake were potentially quite marshy and swampy (*see* Bunting & Warner 1999). The increase in *Larix* which thrives in swampy conditions and will often be among the first colonisers of previously submerged areas supports this hypothesis.

The decline in *Betula* and slight increase in *Pinus strobus* representation in BC2 may indicate intra-species competition. The pattern is broadly contemporaneous with those recorded at Lac Bastien, where Bennett (1987) attributed the decline of *Betula* at *c*. 7980 cal. BP to probable competition with *Pinus strobus*. The establishment of denser woodland environments is inferred from the increased presence of more shade tolerant species such as *Tsuga* and *Fagus* at the BC2-BC3 interface. Our isotopic data also hints at a more closed situation between 308-294cm, before a return to open/arid conditions again. The continued presence of open indicators (*Ambrosia*, *Artemisia*, *Chenopodium* and Poaceae) implies that gaps still exist in the environment surrounding the kettle at this point. The increased representation of *Lycopodiaceae* undiff., which is associated with the perimeters of wooded areas, suggests that the proximity of the woodland to the kettle basin may have been closer during this period. In turn, this may also imply a shift in local hydrological conditions changing the nature and size of the basin. The presence of *Isoetes* indicates that the basin may have expanded at this stage and consequently encroached into the margins of the forest.

The incidence of *Isoetes* increases marginally during BC3: indication of the continued existence of an expanded body of open water. The elevated representation of *Nuphar* and *Equisetum* at the top of the zone, however, points to the presence of aquatic plants and potentially varied habitats within the kettle. Taken together with the variable presence of *Lycopodiaceae* undiff. and Cyperaceae, this implies a certain amount of fluctuation in the size and depth of the water body 8200-7800 cal. BP. Similar patterns are also apparent within the woodland vegetation, with quite dynamic changes in the arboreal environment evident. *Pinus* undiff. becomes even more dominant to the detriment of the majority of the other forest taxa. Only *Tsuga*, *Abies* and *Fraxinus* appear, albeit marginally, to have benefited from this change in composition.

Given the relative stability of Holocene $\delta^{13}C_{air}$ and atmospheric CO_2 concentrations (Elsig *et al*. 2009), and the removal of non-organic pedogenic carbonates during the pre-treatment of samples from this core, the pronounced increases in $\delta^{13}C$ observed at 332-316cm and again and to a lesser extent at 286cm likely reflect environmental changes affecting vegetation in and near to the kettle. One major factor affecting δ^{13}C of terrestrial plants is water stress, which can raise plant δ^{13}C by more than 5‰ (Farquhar, Ehleringer & Hubick 1989). The generally waterlogged conditions within the kettle mean that the supply of groundwater should not have been a problem unless constrained by permafrost conditions – unlikely but not impossible over the duration of the sequence at this latitude. A contribution from aquatic plants to the two peaks above –23‰ cannot be completely ruled out. Freshwater aquatic plants are known to vary widely in δ^{13}C (e.g., Fry & Sher 1984) and may additionally be affected by a variety of environmental variables, such as changes in CO_2 concentration within the lake water (*see* review in Leng *et al*. 2006). Yet the low incidence of aquatic plant pollen (<5%) throughout the core sequence is consistent with a mostly shallow lake that may have largely dried out seasonally. Based on the available evidence, the peaks appear to be primarily reflecting changes in the terrestrial ecosystem in the Balsam Creek catchment area.

It has been shown (Kohn 2010) that in C_3 plants δ^{13}C values above –23‰ are generally restricted to extremely arid (desert) environments; however, their occurrence within *Pinus* sp. dominated montane (i.e., cool arid) settings has also been recorded (e.g., DeLucia & Schlesinger 1991). A change in aridity, potentially brought about by changes in the strength of katabatic winds blowing out from the degrading ice sheet, may have manifested in vegetation growing within the broader catchment of Balsam Creek as an increase in δ^{13}C. Interestingly, the oldest of the δ^{13}C deviations (332-316cm) crosses three sedimentary contexts identified within Unit 6 (Table 1). This suggests that sedimentary changes may have occurred independently, or that they were out of phase with the climatic changes at this point in the sequence. The more or less static δ^{13}C values of –27‰ above 154cm (pollen zones BC8 to BC10) can be interpreted as indicating good wet and stable growing conditions in the Balsam Creek kettle. The period before this is characterised by slightly higher δ^{13}C values of *c*. –25.5‰, and in the absence of major changes in the pollen sequence across this boundary, this likely reflects an environmental difference characterised by colder and drier conditions.

CZ1-6 and the lower *c*. 20cm of CZ7 correlate to the Early Holocene and are characterised by oscillating frequencies in the Ca/Al, Ti/Al, Rb/Al, Sr/Al, Zr/Al and Fe/Al ratios. These signatures likely reflect phases of landscape instability and sediment influx into the kettle. The laminations of clay and silt at depths of 314-326.5cm, 238-345.5cm, 349-353cm and 359-362cm appear to be linked to variations in Si/Ti, Ti/Al, Rb/Al, Sr/Al, Zr/Al and Fe/Al ratios. Alternate phasing of detrital sediment influx and lake stability is also indicated by the inversely varying oscillations in organic content and mineral residue bulk sediment analyses.

Overall, bulk organic δ^{13}C values from 162cm to the base of the core (encompassing most of sedimentary Unit 5 and all of Unit 6; BC1 to BC6 and part of BC7) suggest more arid growing conditions to those experienced above this level. Our age-depth model assigns ages to two prominent increases in δ^{13}C between 332-316cm (modelled mean age-range: 8475-8040 cal. BP) and 286cm (modelled mean age: 7645 cal. BP) (*also see* Lewis 2008; McCarthy & McAndrews 2010). Linkage to the 8.2 Cold Event is likely for the 332-316cm peak, though the time range in our data more closely corresponds with the extended period of Early Holocene climatic anomalies identified in the GISP2 core (Rohling & Pälike 2005). Indeed, the existence of more than one cooling event during the period *c*. 9000-8000 cal. BP has been observed in comparable western hemisphere studies (e.g., Hu *et al*. 1999; Keigwin *et al*. 2005;

Lutz 2007). The existence of another cold interval during the subsequent millennium has not been identified in those records; however such signals have appeared in the European sequence e.g., at *c*. 7100 cal. BP, also from a kettle lake core (Lamentowicz *et al*. 2008). The Balsam Creek data would appear to support the position that dramatic dips in Early Holocene climate may have been accompanied by secondary cold-arid periods.

It is notable that both of these intervals also correspond closely with the two principal spikes in cryptotephra identified at 284cm and 325cm and show broad correspondence to phases of reduced PC1 values in the XRF data (Figure 7). The upper-most of these intervals is attributed to ash from the series of pyroclastic eruptions of Mount Mazama *c*. 7600 years ago. Within our core the modelled age of the deposits containing the Mazama ash ranges 7660-7430 cal. BP (mean age: 7580 cal. BP). This overlaps with the date presented by Zdanowicz *et al*. (1999) of 7627±150 cal. BP and the age range proposed by Egan, Staff & Blackford (2015) of 7682-7584 cal. BP. We considered and rejected the possibility that the lower spike could be a result of density-induced settling within the profile. The Llao Rock precursor eruption was thought to be a likely candidate for the deeper peak; however, the modelled age for the BCK-325 accumulation, together with the variance in cryptotephra geochemistry, currently point to a discrete as yet unknown volcanic event occurred during this period of environmental deterioration.

By the mid-point of BC3 and continuing into BC4 *Pinus* undiff. is significantly less dominant in the woodland environment; with both *Picea* and *Betula* initially recovering to some degree. A very abrupt increase in *Pinus strobus* at the BC3-BC4 transition (*c*. 298cm: 7800 cal. BP) signifies the colonisation of the surrounding forests by this species and the initiation of a major change in the woodland dynamics. This is a widely recognised vegetation succession throughout the region (e.g., Liu 1990; Fuller 1997). The kettle basin environment also shows signs of change at this time with a reduction in the aquatic and spore species during BC4. The correlation between the 284cm ash concentration and the second $\delta^{13}C$ peak within this unit makes a purely taphonomic argument even less convincing. The detection of the ash and its correlation to these signals suggests that harsher climates may be a first indication of the possible effects of ash fall-out on this landscape.

The continued presence of the open indicators *Ambrosia*, *Artemisia* and Poaceae imply that open areas still existed in what appears to have been a mosaic of boreal and deciduous woodland environments. With more dense stands occupied by shade tolerant species such as *Acer*, *Tsuga* and *Fagus* and more open shrubby environments, potentially at the very edges of the basin, inhabited by *Betula*, *Corylus and Larix,* with some herbaceous flora in the understorey. The elevated presence of *Pinus Strobus* around Balsam Creek as the Early Holocene progresses (BC4-BC5 boundary) probably reflects the warmer regional climate during this time. The increased presence of other thermophiles such as *Fagus* during BC4-BC5 (and *Tsuga* later in BC6) support this change in climate, which is also reflected in bulk organic $\delta^{13}C$ signals that settle at *c*. –25.5‰ or lower for most of BC5 to BC7.

5.2 Mid-Holocene – Vegetation zones (BC6 to BC7)

The Mid-Holocene is represented by CZ7 in the XRF data, wherein low-moderate amplitude oscillations in Fe/Al, Rb/Al, Sr/Al and Zr/Al are interpreted as likely representing the physically weathered products of the local quaternary geology. From the end of BC5 and throughout the remainder of the sequence some degree of shrub/grassland (*Corylus avellana*/Poaceae) expansion is evident around Balsam Creek. The diversity in open areas appears diminished from BC6 onwards, with only *Artemisia* present throughout the Mid-

Holocene communities. Cyperaceae indicates that the areas adjacent to the kettle are still marshy and remained so throughout the Mid-Holocene; however, the hydrological conditions appear to have fluctuated. In the early stages of BC6 only the shallow water-associated *Nuphar* is present, while by the BC6-BC7 transition (*c*. 4795 cal. BP) *Isoetes* reappears, synchronous with an increase in the presence of *Nuphar*, hinting at a certain amount of environmental diversity within the water body by this time. Although diatoms are not present in every sample, when they are present, indications are of a general increase in occurrence as the Mid-Holocene progresses. This may relate to changes in the nitrogen and phosphorus ratio in the water body, and in turn imply changes in localised hydrological conditions, such as surface run-off. Unlike other regional lake studies – such as Liu (1990) in which *Pinus strobus* became the dominant taxon from *c*. 7400 cal. BP onwards at Lake Nina, and Fuller (1997) where both *Tsuga* and *Fagus* are much more prominent in the landscape for an extended period of time at Graham Lake – the impact of any climate warming on the vegetation surrounding Balsam Creek appears to have been less pronounced and shorter in duration. *Pinus strobus* is the only dominant forest taxon during BC4, retreating during BC5 as *Pinus* undiff. returns to dominance. Expansion of *Tsuga* and *Fagus* communities, while continuous from this point on, is minimal, though a muted peak and subsequent decline in *Tsuga* is noted (*see* Haas & McAndrew 2000).

The BC6-BC7 transition also appears to mark a significant period in the terrestrial vegetation succession at Balsam Creek, with changes inside the basin potentially related to wider shifting conditions taking place in the adjacent landscape. The return of boreal species such as *Abies* and *Picea* at the termination of BC6 is indicative of colder more arid conditions across the region. It is feasible that if the vegetation succession at Balsam Creek had been altered to a lesser degree by regional warming during the Hypsithermal this may have facilitated a more rapid re-establishment of boreal elements once cooling had begun. The dynamics of the woodland before this time also change and stable succession is evident within the forested environment. *Pinus strobus* stabilises after BC7 and remains a relatively constant element of the woodland to the top of the profile. Similarly, the *Pinus* undiff. population, while remaining dominant, is (albeit marginally) steadily declining throughout the remainder of the sequence. Conversely, *Betula* is becoming an increasingly more dominant element throughout the Mid-Holocene. This increase in the shade intolerant birch potentially indicates a gradual return to less densely populated stands of woodland as the Mid-Holocene continued. This may be reflected in the populations of *Tsuga*, *Alnus*, *Quercus* and *Ulmus*, all of which are declining from the BC6-BC7 transition onwards.

5.3 Late Holocene – Vegetation zones (BC8 to BC10)

The Late Holocene is represented by the upper part of CZ7. Between 63cm and 20cm increasing Ca/Al and Ca/Sr values correlate well to increasing organic content values, but are uncoupled from $CaCO_3$ content. This suggests that increasing Ca content was a factor of both hydrological conditions and biological activity in the basin during this period, perhaps by Calcium Oxalate-forming lichens and mosses. In general, the vegetation succession evident during the Late Holocene is a continuation of that which started in the Mid-Holocene. Stable bulk organic $\delta^{13}C$ values, mostly around –27‰, from the start of BC8 until the top of the core suggest the establishment of a stable forest ecosystem, balanced with increased aquatic productivity marked clearly in the aquatic plant pollen record, particularly *Nuphar* sp. An uptake in aquatic productivity at this time is also supported by increased diatom abundance in pollen samples throughout the upper sections of the core (section

4.6.8). Significant changes from deeper in the sequence include an increased presence of *Abies* and *Picea*, suggesting an increase in these boreal elements within the forest community. The marginal increase of *Salix* and of *Corylus avellana* indicate an expansion of/or diversification within the shrub environment. The continuation of *Betula* as a major element of the vegetation supports this. Increased Cyperaceae during the Late Holocene suggests that any such an environment may have been quite swampy in nature. The increase in both boreal shade tolerant and shrubby shade intolerant species suggests that a marsh thrived at the open, yet sheltered, margins of the basin and that this was surrounded by a mixed coniferous/deciduous forest. An increase in the open indicator *Ambrosia* is apparent within the Late Holocene portion of the core. Bunting and Warner (1999) have interpreted the presence of *Ambrosia* at the very top of their sequence from the Spiraea wetland kettle in southern Ontario as a signal of landscape management due to the arrival of European settlers. The fact that it is present in the Early Holocene at Balsam Creek, however, and with little other impact evident to the woodland taxa make it difficult to say if this the Late Holocene increase in *Ambrosia* can be put down to anthropogenic or natural (or a mixture of both) causes. While we see no clear evidence for human activity within the Balsam Creek sequence, the record does nonetheless presents interesting possibilities for future investigation in this respect.

5.4 Archaeological potential

Generally poor organic preservation and the near absence of zooarchaeological remains from sites continue to leave discussion about Late Palaeoindian (Eastern Plano) subsistence largely speculative. Early penetration of the newly deglaciated north lands by Late Palaeoindian groups is widely assumed to have come about in pursuit of migratory birds and land herbivores that favoured the widespread but relatively short-lived early open tundra-like vegetation that preceded forest development. The existence of strandline sites is taken as evidence for the relatively high biological productivity of the early lakes. While this remains to be proven, given the rate of habitat change they experienced, there are indications that molluscs, which were adapted to the cold pro-glacial lake conditions, colonized these habitats quickly after deglaciation (e.g., Miller, Karrow & Kalas 1979). It is certainly also possible that deglaciation saw the expansion of species of vertebrate lake-fauna out of southern glacial refugia including, but probably not restricted to, the upper reaches of the Mississippi River system pro-glacial lakes (Wilson & Herbert 1996). This is hinted at by the survival of a variety of lake trout (*Salvelinus namaycush*), the Haliburton Highlands lake trout, which exhibits unusually high levels of genetic diversity and is now unique to a small number of lakes south of North Bay. These stocks are inferred to be interglacial relics. After re-colonizing the early deglacial lakes, they became isolated in individual basins during the rapid decline in post-Algonquin water levels (Ihssen *et al*. 1988; CFM Lewis *pers. comm*. to R Rabett 2010). Such zooarchaeological evidence as currently exists comes largely from the western GLB region and suggests that rather than being initially specialized as large-game hunters in the manner of their Plano antecedents on the western plains, the Late Palaeoindian arrivals were as diversified in their subsistence economy as those in the subsequent Early (Shield) Archaic period (Kuehn 1998) and geared to exploit a range of different resources where no one individual resource was abundant or reliable enough (*see* Dawson 1983).

The value of kettle lake habitats within post-glacial inter-fluvial or inter-lacustrine environments has rarely been discussed in this context, but their potential significance to

Palaeoindian and later Archaic communities has been argued on the basis of their attractiveness to small and medium-sized game, and to migratory birds (Carmichael 1977; Deller 1979). Our data do not contain any indication of burning within the Balsam Creek sequence that could be construed as an early human presence, but what they do suggest is that vegetative communities within steep-sided kettles, like Balsam Creek (and it is as yet unclear if the areal extent of the kettle is a factor), may have been buffered against the effects of the climatic fluctuation during the onset and establishment of the Holocene. Given the level of organic preservation at Balsam Creek, together with the penchant of early human groups to exploit lakeside environments, future assessment of these landscape features may yield valuable evidence of early human occupation. Kettle lakes may have been natural attractors to game and human pioneers alike.

6. CONCLUSION

The reported sequence from the Balsam Creek kettle lake shows excellent organic preservation and spans a period from the recent past back to *c*. 10,480 cal. BP, commensurate with the onset of post-glacial peat accumulation in this part of the Canadian Shield. The sedimentary sequence provides a substantial new Holocene palaeo-environmental record for north-east Ontario, anchored against an AMS ^{14}C and cryptotephra chronology, which includes evidence of the Mazama climactic eruption and an earlier as yet unidentified eruption. Multi-proxy data demonstrate that this setting was subject to climatic and environmental changes affecting the region as a whole. There are several points of agreement between the Balsam Creek sequence and external records that situate this site within wider trends in landscape succession (e.g., in the initial dominance and subsequent decline of *Picea* between pollen zones BC1 and BC4; the decline of *Betula* in BC2; and the abrupt increase in *Pinus* across the BC3-BC4 transition). DEM shoreline data suggests that the kettle was probably last flooded during a lake phase that we have tentatively ascribed to the Payette. There is no sign that subsequent lake phases inundated this location.

Evidence obtained through the lithological, pollen and bulk organic δ^{13}C analyses indicates that the deposition of Unit 6 was marked by two intervals during which local vegetation growth was particularly affected. The modelled dates for these intervals are 8475-8040 cal. BP (332-316cm) and 7645 cal. BP (286cm) (Supplementary Table 1). The older of the two intervals may equate to the period of basin closure and subsequent onset of the Nipissing phases of post-Algonquin lake evolution and linkage to a period of cold anomalies around the 8.2 Cold Event is considered likely. The later interval is potentially documenting a separate Early Holocene aridity pulse. The exact nature of the relationship between these two pulses and the associated spikes in cryptotephra is unclear, though it could suggest a link between volcanic activity and the onset or the deepening of more arid conditions during both intervals.

Above Unit 6 our data portray comparatively stable conditions throughout the rest of the cored profile, with fewer indications of dramatic changes in species representation around the kettle compared to what is seen at other sites. We observed that persistence in the vegetation community at Balsam Creek is notably analogous to that seen in the (smaller) Spiraea wetland kettle (Bunting & Warner 1999) *c*. 360km to the south. The data presented herein clearly demonstrate that changes within the Balsam Creek kettle were linked to wider landscape change; however, they also lead to the possibility that kettle basins may have aided in the establishment and persistence of micro-environments which, though existing in isolation, were to some degree less susceptible to the effects of regional disturbance than the landscapes in which they sat. This characteristic could have presented a possible aid to the pioneering colonisation of the dynamic landscapes of north-east Ontario during the early post-glacial period.

ACKNOWLEDGEMENTS

Principal funding for the research presented in this report was provided through a D.M. McDonald Grants and Awards Fund grant to RR, and a Newton Trust Small Research Grant, awarded to RS and RR. We would like to thank Ron Vaillancourt (Ontario Ministry of Natural Resources, North Bay District) for permission to collect sediment core profiles from the study location. Thorsten Kahlert and Shawn O'Donnell provided insights into digital elevation modelling and palaeoenvironmental interpretation, respectively. RR thanks Ben Verzijlenberg and Tina Rabett for their assistance prospecting for and collecting the cores used in this study. AJEP thanks Steve Boreham and Chris Rolfe for technical assistance with collecting the loss on ignition and magnetic susceptibility data. DS thanks Rachel Patterson for her assistance with pollen preparation. We greatly appreciate the critical and constructive assessments provided by two anonymous reviewers and the OQ editor on an earlier version of this article. The DEMs presented here contain information that is licensed under the Open Government License Ontario and that can be freely downloaded at following address: https://www.javacoeapp.lrc.gov.on.ca/geonetwork/srv/en/main.home).

The authors declare that they have no competing interests in publishing this article.

REFERENCES

Anderson, RY, Nuhfer, EB, Dean WE 1984. Sinking of volcanic ash in uncompacted sediment in Williams Lake, Washington. *Science* 225: 505-508.

Anderson, TW, Lewis, CFM, Mott, RJ 2001. AMS-revised radiocarbon ages at Turtle Lake, North Bay-Mattawa area, Ontario: Implications for the deglacial history of the Great Lakes region. 27th Annual Scientific Meeting of the Canadian Geophysical Union, Ottawa, Ontario, p. 51.

Anderson, TW 2002. Pollen stratigraphy and vegetation history, Sheguiandah archaeological site, in *The Sheguiandah Site: Archaeological, Geological and Palaeobotanical Studies at a Paleoindian site on Manitoulin Island, Ontario*, ed. P.J. Julig. Mercury Series. Archaeological Survey of Canada Paper 161: 179-194.

Anderson, TW & Lewis, CFM 2002. Upper Great Lakes climate and water-level changes 11 to 7 ka: effect on the Sheguiandah archaeological site, in *The Sheguiandah Site: Archaeological, Geological and Palaeobotanical Studies at a Paleoindian site on Manitoulin Island, Ontario*, ed. P.J. Julig. Mercury Series. Archaeological Survey of Canada Paper 161: 195-234.

Aniceto, K., Moreira-Turcq, P. Cordeiro, R., Quintana, I., Fraizy, P. and Turcq, B. 2014. Hydrological Changes in West Amazonia over the Past 6 Ka Inferred from Geochemical Proxies in the Sediment Record of a Floodplain Lake. *Procedia Earth and Planetary Science* 10: 287-291. DOI: https://doi.org/10.1016/j.proeps.2014.08.065

Bacon, CR 1983. Eruptive history of Mount Mazama and Crater Lake Caldera, Cascade Range, U.S.A. *Journal of Volcanology and Geothermal Research* 18: 57-115.

Bacon, CR & Lanphere, MA 2006. Eruptive history and geochronology of Mount Mazama and the Crater Lake region, Oregon. *GSA Bulletin* 118(11/12): 1331-1359. DOI: https://doi.org/10.1130/B25906.1

Ball, DF 1964. Loss-on-ignition as an estimate of organic matter and organic carbon in non-calcareous soils. *Journal of Soil Science* 15(1): 84-92. DOI: https://doi.org/10.1111/j.1365-2389.1964.tb00247.x

Barnett, PJ & Bajc, AF 2002. Quaternary Geology, in *The Physical Environment of the City of Greater Sudbury. Ontario Geological Survey* Special Vol. 6: 58-59.

Bartlein, PJ, Anderson, PM, Anderson, KH, Edwards, ME, Thompson, RS, Webb, RS, Webb III, T, Whitlock, C 1998. Paleoclimate simulations for North America for the past 21,000 years: Features of the simulated climate and comparisons with paleoenvironmental data. *Quaternary Science Reviews 17*: 549-85. DOI: https://doi.org/10.1016/S0277-3791(98)00012-2

Beierle, B & Bond, J 2002. Density-induced settling of tephra through organic lake sediments. *Journal of Paleolimnology* 28: 433-440.

Bennett, KD 1987. Holocene history of forest trees in southern Ontario. *Canadian Journal of Botany*, 65(9): 1792-1801. DOI: https://doi.org/10.1139/b87-248

Bennett, MR & Glasser, NF 2009. *Glacial Geology: Ice Sheets and Landforms*. Wiley-Blackwell: Chichester.

Blaauw, M & Christen, JA 2011. Flexible paleoclimate age-depth models using and autoregressive gamma process. *Bayesian Analysis* 6: 457-474. DOI: https://doi.org/10.1214/11-BA618

Blockley, SPE, Pyne-O'Donnell, SDF, Lowe, JJ, Matthews, IP, Stone, A, Pollard, AM, Turney, CSM, Molyneux, EG 2005. A new and less destructive laboratory procedure for the physical separation of distal glass tephra shards from sediments. *Quaternary Science Reviews* 24: 1952-1960. DOI: https://doi.org/10.1016/j.quascirev.2004.12.008

Boissonneau, AN 1968. Glacial History of Northeastern Ontario II. The Timiskaming-Algoma Area *Canadian Journal of Earth Sciences* 5(l), 97-109.

Bonafini, M, Pellegrini, M, Ditchfield, P, Pollard, AM 2013. Investigation of the 'canopy effect' in the isotope ecology of temperate woodlands. *Journal of Archaeological Science* 40(11): 3926-3935. DOI: https://doi.org/10.1016/j.jas.2013.03.028

Borchardt, GA, Aruscavage, PJ, Millard, HT 1972. Correlation of the Bishop Ash, a Pleistocene marker bed using instrumental neutron activation analysis. *Journal of Sedimentary Petrology* 42: 301-306. DOI: https://doi.org/10.1306/74D72527-2B21-11D7-8648000102C1865D

Breckenridge, A, Lowell, TV, Fisher, TG, Yu, S 2012. A late Lake Minong transgression in the Lake Superior basin as documented by sediments from Fenton Lake, Ontario. *Journal of Paleolimnology*. DOI: https://doi.org/10.1007/s10933-010-9447-z

Brooks, GR & Medioli, BE 2010. Sub-bottom profiling and coring of sub-basins along the lower French River, Ontario: insights into depositional environments within the North Bay outlet. *Journal of Paleolimnology*. DOI: https://doi.org/10.1007/s10933-010-9414-8

Brooks, GR, Medioli, BE, Telka, AM 2010. Evidence of early Holocene closed-basin conditions in the Huron-Georgian basins from within the North Bay outlet of the upper Great Lakes. *Journal of Paleoliminology* DOI: https://doi.org/10.1007/s10933-010-9408-6

Bryant, VM Jr. & Holloway, RG 1985. *Pollen Records of Late-Quaternary North American Sediments*. American Association of Stratigraphic Palynologists. Hart Graphics Inc.: Austin.

Bunting, MJ & Warner, BG 1999. Late Quaternary vegetation dynamics and hydroseral development in a shrub swamp in southern Ontario, Canada. *Canadian Journal of Earth Sciences* 36: 1603-1616.

Burwasser, GJ 1979. *Quaternary Geology of the Sudbury Basin Area: District of Sudbury*. Report 18 Ontario Geological Survey, Ministry of Natural Resources: Toronto.

Carmichael, DL 1977. Preliminary archeological survey of Illinois uplands and some behavioral implications. *Mid-Continental Journal of Archaeology* 2(2): 219-251.

Chapman, LJ 1954. An Outlet of Lake Algonquin at Fossmill, Ontario, *Geological Association of Canada Proceedings* 6(2): 61-68.

Chapman, LJ 1975. *The Physiography of the Georgian Bay-Ottawa Valley Area of Southern Ontario*; Ontario Div. Mines, GR 128, 35p. Accompanied by Map 2228, scale: 1 inch to 4 miles or 1:253,440.

Clarke, GKC, Leverington, DW, Teller, JT, Dyke, AS 2004. Paleohydraulics of the last outburst flood from glacial Lake Agassiz and the 8200 BP cold event. *Quaternary Science Reviews* 23: 389-407. DOI: https://doi.org/10.1016/j.quascirev.2003.06.004.

Cohen, AS 2003. *Paleolimnology: the History and Evolution of Lake Systems*. Oxford University Press: Oxford.

Cowan, WR 1985. Deglacial Great Lakes shorelines at Ste. Marie, Ontario, in *Quaternary evolution of the Great Lakes*, Karrow, P.F. & Calkin, PE (eds.). *Geological Association of Canada* Special Paper 30: 33-37.

Cowan, WR & Broster, BE 1988. Quaternary geology of the Sault Ste. Marie area, District of Algoma, Ontario. Ontario Geological Survey Map P.3104, Geological Series Preliminary Map, scale 1:100,000.Geology 1976.

Dawson, KCA 1983. Prehistory of the interior forest of Northern Ontario, in *Boreal Forest Adaptations: The Northern Algonkians*, (ed.) Steegmann, Jr., AT. Plenum Press: New York, pp. 55-84.

Daigneault, R-A & Occhietti, S 2006. Les moraines du massif Algonquin, Ontario, au début du Dryas récent, et corrélation avec la Moraine de Saint-Narcisse. *Géographie physique et Quaternaire* 602: 103-118. DOI: https://doi.org/10.7202/016823ar

Daubois, V, Roy, M, Veillette, JJ, Ménard, M 2015. The drainage of Lake Ojibway in glaciolacustrine sediments of northern Ontario and Quebec, Canada. *Boreas* 44(2): 305-318. DOI: https://doi.org/10.1111/bor.12101

Deller, DB 1979. Paleo-Indian reconnaissance in the counties of Lambton and Middlesex, Ontario. *Ontario Archaeology* 32: 3-20.

Delucia, EH & Schlesinger, WH 1991. Resource-use efficiency and drought tolerance in adjacent Great Basin and sierran plants. Ecology 72(1): 51-58. DOI: https://doi.org/10.2307/1938901

Drucker, DG & Bocherens, H 2009. Carbon stable isotopes of mammal bones as tracers of canopy development and habitat use in temperate and boreal contexts, in *Forest Canopies: Forest Production, Ecosystem Health, and Climate Conditions*, Creighton, JD & Roney, PJ eds.) Nova Science Publishers, Inc., pp. 103-109.

Dyke, AS, Vincent, J-S, Andrews, JT, Dredge, LA, Cowan, WR 1989. The Laurentide Ice Sheet and an introduction to the Quaternary geology of the Canadian Shield, in *Quaternary Geology of Canada and Greenland*, Fulton, JR (ed.) Geological Society of America, Vol. K1: 175-312. DOI: https://doi.org/10.1130/DNAG-GNA-K1

Egan, J, Staff, R, Blackford, J 2015. A revised age estimate of the Holocene Plinian eruption of Mount Mazama, Oregon using Bayesian statistical modelling. *The Holocene* 25: 1054-1067. DOI: https://doi.org/10.1177/0959683615576230

Elsig, J, Schmitt, J, Leuenberger, D, Schneider, R, Eyer, M, Leuenberger, M, Joos, F, Fischer, H, Stocker, TF 2009. Stable isotope constraints on Holocene carbon cycle changes from an Antarctic ice core. *Nature* 461: 507-510. DOI: https://doi.org/10.1038/nature08393

Enache, MD & Cumming, BF 2006. The morphological and optical properties of volcanic glass: a tool to assess density-induced vertical migration of tephra in sediment cores. *Journal of Paleolimnology* 35: 661-667. DOI: https://doi.org/10.1007/s10933-005-3604-9

Farquhar GD, Ehleringer JR, Hubick KT 1989. Carbon isotope discrimination and photosynthesis. *Annual Review of Plant Physiology and Plant Molecular Biology* 40: 503-537. DOI: https://doi.org/10.1146/annurev.pp.40.060189.002443

Faegri, K & Iversen, J 1989. Textbook of pollen analysis (4^{th} edition by Faegri, K, Kaland, PE & Krzywinski, K). Wiley, Chichester.

Foit, FF Jr. & Mehringer, PJ Jr. 2016. Holocene tephra stratigraphy in four lakes in southeastern Oregon and northwestern Nevada, USA. Quaternary Research 85(2): 218-226. DOI: https://doi.org/10.1016/j.yqres.2015.12.008

Fry, B & Sherr, EB 1984. $\delta^{13}C$ measurements as indicators of carbon flow in marine and freshwater ecosystems. *Contributions to Marine Science* 27: 13-47.

Fuller, JL 1997. Holocene forest dynamics in southern Ontario, Canada: fine-resolution pollen data. *Canadian Journal of Botany* 75: 1714-1727.

Gartner, JF 1980. North Bay Area (NTS 31L/SW), Districts of Nipissing and Parry Sound. *Ontario Geological Survey*, Northern Ontario Engineering Geology Terrain Study 101, Accompanied by Maps 5041 and 5044, scale: 1:100000.

Greenman, E.F. 1943. An Early Industry on a Raised Beach near Killarney, Ontario. *American Antiquity* 8(3): 260-265.

Greeman, EF, 1966. Chronology of Sites at Killarney, Canada. *American Antiquity* 31(4): 540-551.

Grimm, EC 2004. Tilia and TG View Version 2.0.2 Illinois State Museum, Research and Collector Center.

Haas, JN & McAndrew, JH 2000. The summer drought related hemlock (*Tsuga canadensis*) decline in Eastern North America 5,700 to 5,100 years ago. In McManus, KA, Shields, KS, Souto DR (eds.) Proceedings: *Symposium on Sustainable Management of Hemlock Ecosystems in Eastern North America*. General Technical Report NE-267. Newtown Square, PA: U.S. Department of Agriculture, Forest Service, Northeastern Forest Experiment Station, p. 81-88.

Haberzettl, T, St-Onge, G, Lajeunesse, P 2010. Multi-proxy records of environmental changes in Hudson Bay and Strait since the final outburst flood of Lake Agassiz–Ojibway. *Marine Geology* 271: 93-105. DOI: https://doi.org/10.1016/j.margeo.2010.01.014

Harrison, JE 1972. Quaternary geology of the North Bay-Mattawa region. *Geological Survey of Canada,* Ottawa, Memoir 10.

Heath, AJ & Karrow, PF 2007. Northernmost(?) Glacial Lake Algonquin series shorelines, Sudbury Basin, Ontario. *Journal of Great Lakes Research* 33: 264-78. DOI: https://doi.org/10.3394/0380-1330(2007)33[264:NGLASS]2.0.CO;2

Heiri, O, Lemcke, G, Lotter, AF 2001. Loss on ignition as a method for estimating organic and carbonate content in sediments: Reproducibility and comparability of results. *Journal of Paleolimnology* 25: 101–110. DOI: https://doi.org/10.1023/A:1008119611481

Hu, FS, Slawinski, D, Wright Jr, HE, Ito, E, Johnson, RG, Kelts, KR, McEwan, RF, Boedigheimer, A 1999. Abrupt changes in North American climate during early Holocene times. *Nature* 400: 437-440. DOI: https://doi.org/10.1038/22728

Ihssen, PE, Casselman, JM, Martin, GW, Phillips, RB 1988. Biochemical genetic differentiation of lake trout (*Salvelinus namaycush*) stocks of the Great Lakes region. *Canadian Journal of Fisheries and Aquatic Science*, 45: 1018-29.

Jackson, LJ, Ellis, C, Morgan, AV, McAndrews, JH 2000. Glacial lake levels and Eastern Great Lakes Palaeo-Indians. *Geoarchaeology* 15(5): 415-40. DOI: https://doi.org/10.1002/(SICI)1520-6548(200006)15:5<415::AID-GEA2>3.0.CO;2-2

Julig, PJ 2002. Archaeological conclusions from the Sheguiandah Site research, in *The Sheguiandah Site: Archaeological, Geological and Palaeobotanical Studies at a Paleoindian site on Manitoulin Island, Ontario*, Julig, PJ (ed.). Mercury Series. Archaeological Survey of Canada Paper 161: 297-311.

Julig, PJ & McAndrews, JH 1993. Les cultures Paléoindiennes dans la region des Grands Lacs en Amérique du Nord: contexts Paléoclimatique, géomorphologiques et stratigraphiques. *L'Anthropologie* 97(4): 623-650.

Karrow, PF 2004. Algonquin-Nipissing shorelines, North Bay, Ontario. *Géographie physique et Quaternaire* 58(2–3): 297-304. DOI: https://doi.org/10.7202/013144

Karrow, PF, Anderson, TW, Clarke, AH, Delorme, LD, Sreenivasa, MR 1975. Stratigraphy, Paleontology, and Age of Lake Algonquin Sediments in Southwestern Ontario, Canada. *Quaternary Research* 5: 49-87. DOI: https://doi.org/10.1016/0033-5894(75)90048-4

Keeling, PS 1962. Some Experiments on the Low-Temperature Removal of Carbonaceous Material from Clays. *Clay Minerals Bulletin* 5(28): 155-158. DOI: https://doi.org/10.1180/claymin.1962.005.28.10

Kehew, AE and Brandon Curry, B 2018. *Quaternary Glaciation of the Great Lakes Region: Process, Landforms, Sediments and Chronology*. *The Geological Society of America*, Special Paper 530.

Keigwin, LD, Sachs, PJ, Rosenthal, Y, Boyle EA 2005. The 8200 year B.P. event in the slope water system, western subpolar North Atlantic. Paleooceanography 20: PA2003. DOI: https://doi.org/10.1029/2004PA001074

Ketchum, JWF & Davidson, A 2000. Crustal architecture and tectonic assembly of the Central Gneiss Belt, southwestern Grenville Province, Canada: a new interpretation. Canadian Journal of Earth Sciences 37: 217-234. DOI: https://doi.org/10.1139/e98-099

Kohn, MJ 2010. Carbon isotope compositions of terrestrial C3 plants as indicators of (paleo)ecology and (paleo)climate. *PNAS* 107(46): 19691-95. https://doi.org/10.1073/pnas.1004933107

Kor, PSG 1991. The Quaternary Geology of the Parry Sound-Sundridge Area, Central Ontario. *Ontario Geological Survey*, Open File Report 5796.

Kuehn, SR 1998. New evidence for Late Paleoindian-Early Archaic subsistence behavior in the western Great Lakes. *American Antiquity* 63(3): 457-76. DOI: https://doi.org/10.2307/2694630

Lamentowicz, M, Obremska, M, Mitchell, EAD 2008. Autogenic succession, land-use change, and climatic influences on the Holocene development of a kettle-hole mire in Northern Poland. *Review of Palaeobotany and Palynology* 151: 21–40. DOI: https://doi.org/10.1016/j.revpalbo.2008.01.009

Lee, TE 1957. The antiquity of the Sheguiandah site. *The Canadian Field-Naturalist* 71: 117-147.

Lee, HA 1960. Late glacial and postglacial Hudson Bay sea episode. *Science* 131(3413): 1609-11.DOI: https://doi.org/10.1126/science.131.3413.1609

Lehman, JT 1975. Reconstructing the rate of accumulation of lake sediment: the effect of sediment focusing. *Quaternary Research* 5: 541-550. DOI: https://doi.org/10.1016/0033-5894(75)90015-0

Leng, MJ, Lamb, AL, Heaton, THE, Marshall, JD, Wolfe, BB, Jones, MD, Holmes, JA 2006. Isotopes in lake sediments, in *Isotopes in Palaeoenvironmental Research*, Leng, MJ (ed.), Springer Netherlands, pp. 147-184. DOI: https://doi.org/10.1007/1-4020-2504-1

Leverett, F and Taylor, FB 1915. The Pleistocene of Indiana and Michigan and the history of the Great Lakes. US Geological Survey Monograph 53. Washington DC, USGS.

Lewis, CFM 2008. Dry climate disconnected the Laurentian Great Lakes. *EOS* 89(52): 541-552.

Lewis, CFM & Anderson, TW 1989. Oscillations of levels and cool phases of the Laurentian Great Lakes caused by inflows from glacial Lakes Agassiz and Barlow-Ojibway. *Journal of Paleolimnology* 2: 99-146.

Lewis, CFM & Anderson, TW 2012. The sedimentary and palynological records of Serpent River Bog, and revised early Holocene lake-level changes in the Lake Huron and Georgian Bay region. *Journal of Paleolimnology* 47: 391-410. DOI: https://doi.org/10.1007/s10933-012-9595-4

Lewis, CFM, Moore, TC Jr, Rea, DK, Dettman, DL, Smith, AM, Mayer, LA 1994. Lakes of the Huron Basin: their record of runoff from the Laurentide ice sheet. *Quaternary Science Reviews* 13: 891-922. DOI: https://doi.org/10.1016/0277-3791(94)90008-6

Lewis, CFM, Miller, AAL, Levacc, E, Pipera, DJW, Sonnichsen, GV 2012. Lake Agassiz outburst age and routing by Labrador Current and the 8.2 cal. ka cold event. *Quaternary International* 260: 83-97. DOI: https://doi.org/10.1016/j.quaint.2011.08.023

Lewis, CFM, King, JW, Blasco, SM, Brooks, GR, Coakley, JP, Croley II, TE, Dettman, DL, Edwards, TWD., Heil Jr., CW, Hubeny, JB, Laird, KR, McAndrews, JH, McCarthy, FMG, Medioli, BE, Moore Jr., TC, Rea, DK, Smith, AJ 2008. Dry climate disconnected the Laurentian Great Lakes. *Eos* 89(52): 541-52. DOI: https://doi.org/10.1029/2008EO520001

Liu, K-B 1990. Holocene paleoecology of the boreal forest and Great Lakes-St. Lawrence forest in northern Ontario. *Ecological Monographs* 60(2): 179-212. DOI: https://doi.org/10.2307/1943044

Lowell, TV, Larson, GJ, Hughes, JD, Denton, GH 1999. Age verification of the Lake Gribben forest bed and the Younger Dryas advance of the Laurentide Ice Sheet. *Canadian Journal of Earth Sciences* 36: 383-393.

Löwermark L, Chen H-F, Yang T-N, Kylander M, Yu E-F, Hsu Y-W, Lee T-Q, Song S-R, Jarvis S. 2011. Normalizing XRF-scanner data: a cautionary note on the interpretation of high resolution records from organic-rich lakes. *Journal of Asian Earth Science* 40: 1250-1256. DOI: https://doi.org/10.1016/j.jseaes.2010.06.002

Lumbers, SB 1971. Ontario Department of Mines. Geological Report 94: Geology of the North Bay Area. Districts of Nipissing and Parry Sound.

Lutz, B, Wiles, G, Lowell, T, Michaels, J 2007. The 8.2-ka abrupt climate change event in Brown's Lake, northeast Ohio. *Quaternary Research* 67: 292-96. DOI: https://doi.org/10.1016/j.yqres.2006.08.007

McAndrews, JH 1997. Pollen analysis of a sediment core from a bog adjacent to the Fisher site, in *The Fisher Site: Archaeological, Geological and Paleobotanical Studies at an Early*

Paleo-Indian Site in Southern Ontario, Canada, Storck, P (ed.) Memoirs Museum of Anthropology, University of Michigan No. 30, pp. 295-297.

McAndrews, JH, Berti, AA, Norris, G 1973. Key to Quaternary Pollen and Spores of the Great Lake Region. Royal Ontario Museum: Toronto.

McCarthy, F & McAndrews J 2010a. Early Holocene drought in the Laurentian Great Lakes basin caused hydrologic closure of Georgian Bay. *Journal of Paleolimnology*. DOI: https://doi.org/10.1007/s10933-010-9410-z

McCarthy, F, Tiffin, S, Sarvis, A, McAndrews, J, Blasco, S. 2010. Early Holocene brackish closed basin conditions in Georgian Bay, Ontario, Canada: microfossil (thecamoebian and pollen) evidence. *Journal of Paleolimnology*. DOI https://doi.org/10.1007/s10933-010-9415-7

Miller, BB, Karrow, PF, Kalas, LL 1979. Late Quaternary mollusks from Glacial Lake Algonquin, Nipissing and transitional sediments from Southwestern Ontario, Canada. *Quaternary Research* 11: 93-112. DOI: https://doi.org/10.1016/0033-5894(79)90071-1

Ministry of Natural Resources and Forestry (MNRF) 2016. Central Ontario Orthophotography Project (COOP) 2016 Digital Elevation Model. Ontario Ministry of Natural Resources and Forestry, Land Information Ontario, Peterborough, Ontario.

Miousse, L, Bhiry, N, Lavoie, M 2003. Isolation and water-level fluctuations of Lake Kachishayoot, Northern Québec, Canada. *Quaternary Research* 60, 149-61.

Moore Jr. TC, Walker, JGC, Rea, DK, Lewis, CFM, Shanne, LCK, Smith, AJ 2000. The Younger Dryas interval and outflow from the Laurentide ice sheet. *Paleoceanography* 15(1): 9-18. DOI: https://doi.org/10.1029/1999PA000437

Mott, RJ & Farley-Gill, LD 1978. A late-Quaternary pollen profile from Woodstock, Ontario. *Canadian Journal of Earth Science* 15: 1101-1111.

Mott, RJ & Farley-Gill, LD 1981. Two late Quaternary pollen profiles from Gatineau Park, Quebec. *Geological Survey of Canada Special Paper* No. 80-31.

Mulligan, RPM, Eyles, CH, Bajc, AF 2018. Stratigraphic analysis of Late Wisconsin and Holocene glaciolacustrine deposits exposed along the Nottawasaga River, southern Ontario, Canada. *Canadian Journal of Earth Sciences* DOI: https://doi.org/10.1139/cjes-2017-0081

Occhietti, S 2007. The Saint-Narcisse morainic complex and early Younger Dryas events on the southeastern margin of the Laurentide Ice Sheet. *Géographie Physique et Quaternaire*, 61(2-3): 89-117. DOI: https://doi.org/10.7202/038987ar

O'Leary MH 1988. Carbon isotopes in photosynthesis. *BioScience* 38: 328-335.

O'Shea, JM & Meadows, GA 2009. Evidence for early hunters beneath the Great Lakes. *PNAS* 106(25): 10120-10123. DOI: https://doi.org/10.1073/pnas.0902785106

O'Shea, JM, Lemke, AK, Sonnenburg, EP, Reynolds, RG, Abbott, BD 2014. A 9,000-year-old caribou hunting structure beneath Lake Huron. *PNAS* 111(19): 6911-15. DOI: https://doi.org/10.1073/pnas.1404404111

Phillips, BAM 1988. Paleogeographic reconstruction of shoreline archaeological sites around Thunder Bay, Ontario. *Geoarchaeology* 3(2): 127-138. DOI: https://doi.org/10.1002/gea.3340030204

Phillips, BAM 1993. A time-space model for the distribution of shoreline archaeological sites in the Lake Superior Basin. *Geoarchaeology* 8(2): 87-107. DOI: https://doi.org/10.1002/gea.3340080203

Pyne-O'Donnell, SDF, Hughes, PDM, Froese, DG, Jensen, BJL, Kuehn, SC, Mallon, G, Amesbury, MJ, Charman, DJ, Daley, TJ, Loader, NJ, Mauquoy, D, Street-Perrott, FA, Woodman-Ralph, J 2012. High-precision ultradistal Holocene tephrochronology in North America. *Quaternary Science Reviews* 52: 6-11. DOI: https://doi.org/10.1016/j.quascirev.2012.07.024

Reimer, PJ, Bard, E, Bayliss, A, Beck, JW, Blackwel, PG, Bronk Ramsey, C, Buck, CE, Hai Cheng, Edwards, RL, Friedrich, M, Grootes, PM, Guilderson, TP, Haflidason, H, Hajdas, I, Hatté, C, Heaton, TJ, Hoffmann, DL, Hogg, AG, Hughen, KA, Kaiser, KF, Kromer, B, Manning, SW, Niu, M, Reimer, RW, Richards, DA, Scott, EM, Southon, JR, Staff, RA, Turney, CSM, van der Plicht, J 2013. IntCal13 and Marine13 radiocarbon age calibration curves 0–50,000 years cal BP. *Radiocarbon* 55(4): 1869-1887. DOI: https://doi.org/10.2458/azu_js_rc.55.16947

Richter, TO, van der Gaast, S, Koster, B, Vaars, A, Gieles, R, de Stigter, HC, De Haas, H, van Weering, TCE 2006. The Avaatech XRF Core Scanner: technical description and applications to NE Atlantic sediments. *Geological Society*, London, Special Publications, 267: 39–50.

Ritchie, JC 1987. *Postglacial Vegetation of Canada*. Cambridge University Press: Cambridge.

Rohling, EJ & Pälike, H 2005. Centennial-scale climate cooling with a sudden cold event around 8,200 years ago. *Nature* 434: 975-979.

Rothwell, RG & Croudace, IW 2015. Twenty years of XRF core scanning marine sediments: What do geochemical proxies tell us? in *Micro-XRF Studies of Sediment Cores applications of a non-destructive tool for the environmental sciences*, Croudace, IW & Rothwell, RG (eds.). Springer: Netherlands. DOI: https://doi.org/10.1007/978-94-017-9849-5

Roy, M, Dell'Oste, F, Veillette, JJ, de Vernal, A, Hélie, J-F, Parent, M 2011. Insights on the events surrounding the final drainage of Lake Ojibway based on James Bay stratigraphic sequences. *Quaternary Science Reviews* 30: 682-692. DOI: https://doi.org/10.1016/j.quascirev.2010.12.008

Saarnisto, M 1974. The deglaciation history of the Lake Superior region and its climatic implications. *Quaternary Research* 4, 316-339. DOI: https://doi.org/10.1016/0033-5894(74)90019-2

Sage, RF, Wedin, DA, Li, M. 1999. The biogeography of C_4 photosynthesis: patterns and controlling factors, in *C_4 Plant Biology*, Sage, RF and Monson, RK (eds.), San Diego Academic Press, pp. 313-373.

Schaetzl, RJ, Drzyzga, SA, Weisenborn, BN, Kincare, KA, Lepczyk, XC, Shein, K, Dowd, CM, Linker, J 2002. Measurement, correlation and mapping glacial lake Algonquin shorelines in Northern Michigan. *Annals of the Association of American Geographers* 92(3): 399-415.

Schiff, SL, Aravena, R, Trumbore, SE, Hinton, MJ, Elgood, R, Dillon, PJ 1997. Export of DOC from forested catchments on the Precambrian Shield of Central Ontario: Clues from ^{13}C and ^{14}C. *Biogeochemistry* 36: 43–65. DOI: https://doi.org/10.1023/A:1005744131385

Shackley M., S. 2011. An Introduction to X-Ray Fluorescence (XRF) Analysis in Archaeology, in *X-Ray Fluorescence Spectrometry (XRF) in Geoarchaeology*, (ed.) Shackley, M. Springer: New York, pp. 7-44.

Spano, NG, Lane, CS, Francis, SW, Johnson, TC 2017. Discovery of Mount Mazama cryptotephra in Lake Superior (North America): Implications and potential applications. *Geology* 45: 1071-1074. DOI: https://doi.org/10.1130/G39394.1

Spencer, JW 1891. Deformation of the Algonquin beach, and birth of Lake Huron. *American Journal of Science* 141: 12-21.

Storck, PL 1982. Palaeo-Indian Settlement Patterns Associated with the Strandline of Glacial Lake Algonquin in Southcentral Ontario. *Canadian Journal of Archaeology* 6: 1-31.

Storck, PL. 1997. *The Fisher Site: Archaeological, Geological and Paleobotanical Studies at an Early Paleo-Indian Site in Southern Ontario, Canada*. Memoirs Museum of Anthropology, University of Michigan No. 30.

Storck, PL 2004. *Journey to the Ice Age: Discovering an Ancient World*. Vancouver: University of British Columbia Press & Royal Ontario Museum.

Stuiver, M & Reimer, P 1993. Extended ^{14}C data base and revised calib 3.0 ^{14}C age calibration program. *Radiocarbon* 35(1): 215-230. DOI: https://doi.org/10.1017/S0033822200013904

Teller, JT 1995. History and drainage of large ice-dammed lakes along the Laurentide ice sheet. *Quaternary International* 28: 83-92. DOI: https://doi.org/10.1016/1040-6182(95)00050-S

Teller, JT, Yang, Z, Boyd, M, Buhay, WM, McMillan, K, Kling, HJ, Telka, AM 2008. Postglacial sedimentary record and history of West Hawk Lake crater, Manitoba. *Journal of Paleolimnology* 40(2): 661-688. DOI: https://doi.org/10.1007/s10933-008-9192-8

Terasmae, J 1979. Radiocarbon dating and palynology of glacial Lake Nipissing deposits at Wasaga Beach, Ontario. *Journal of Great lakes Research* 5(3–4): 292-300. DOI: https://doi.org/10.1016/S0380-1330(79)72155-1

Terasmae, J & Hughes, OL 1960. Glacial Retreat in the North Bay Area, Ontario. *Science* 131: 1444-1446. DOI: https://doi.org/10.1126/science.131.3411.1444

Thompson R, Stober, JC, Turner, GM, Oldfield, F, Bloemendal, J, Dearing, JA, Rummery, TA, 1980. Environmental applications of magnetic measurements. *Science* 207: 481-486. DOI: https://doi.org/10.1126/science.207.4430.481

Veillette, JJ 1988. Déglaciation et évolution des lacs proglaciaires post-Algonquin et Barlow au Témiscamingue, Québec et Ontario. *Géographie physique et Quaternaire* DOI: https://doi.org/10.7202/032706ar

Veillette, JJ 1994. Evolution and paleohydrology of glacial lakes Barlow and Ojibway. *Quaternary Science Reviews* 13: 945-71. DOI: https://doi.org/10.1016/0277-3791(94)90010-8

Warner, BG., Hebda, RJ, Hann, BJ 1984. Postglacial paleoecological history of a cedar swamp, Manitoulin Island, Ontario, Canada. *Palaeogeography, Palaeoclimatology, Palaeoecology* 45: 301-345. DOI: https://doi.org/10.1016/0031-0182(84)90010-5

Weltje, GJ & Tjallingi, R 2008. Calibration of XRF core scanners for quantitative geochemical logging of sediment cores: Theory and application. *Earth and Planetary Science Letters*, 274(3-4): 423-438. DOI: https://doi.org/10.1016/j.epsl.2008.07.054

Wilson, CC & Hebert, PDN 1996. Phylogeographic origins of lake trout (*Salvelinus namaycush*) in eastern North America. *Canadian Journal of Fisheries and Aquatic Science* 53: 2764-2775. DOI: https://doi.org/10.1139/f96-223

Wolfe, BB, Edwards, TWD, Aravena, R, MacDonald, GM 1996. Rapid Holocene hydrologic change along boreal treeline revealed by 513C and 6180 in organic lake sediments, Northwest Territories, Canada. *Journal of Paleolimnology* 15: 171-181. DOI: https://doi.org/10.1007/BF00196779

Yu, Z 2003. Late Quaternary dynamics of tundra and forest vegetation in the southern Niagara Escarpment, Canada. *New Phytologist* 157: 365-390. DOI: https://doi.org/10.1046/j.1469-8137.2003.00678.x

Yu, S-Y, Colman, SM, Lowell, TV, Milne, GA, Fisher, TG, Breckenridge, A, Boyd, M, Teller, JT 2010. Freshwater outburst from Lake Superior as a trigger for the cold event 9300 years ago. *Science* 328: 1262-1266. DOI: https://doi.org/10.1126/science.1187860
Zdanowicz, CM, Zielinski, GA, Germani, MS 1999. Mount Mazama eruption: Calendrical age verified and atmospheric impact assessed. *Geology* 27: 621-624. DOI: https://doi.org/10.1130/0091-7613(1999)027<0621:MMECAV>2.3.CO;2

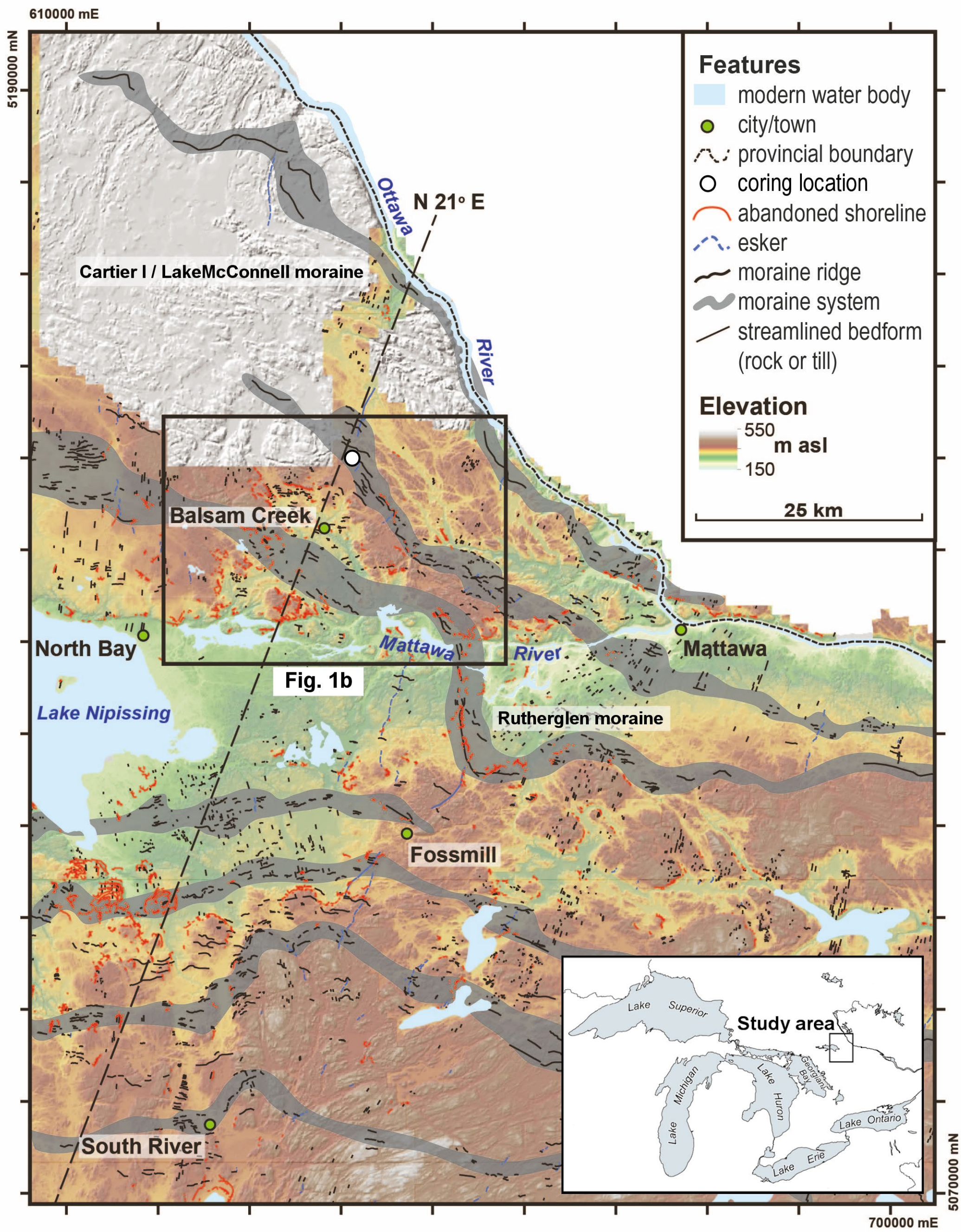

Figure 1a: A regional-scale Digital Elevation Model (DEM; MNRF 2016) showing glacial and glacial lake features, including a preliminary aggregation of moraine ridges (thick black lines) into contemporaneous ice marginal positions (shaded grey areas). The coring location is marked by a white circle; the extent of Figure 1b is shown in the black rectangle (image: R. Mulligan). Inset map (redrawn from Karrow 2004) shows study area relative to the Great Lakes.

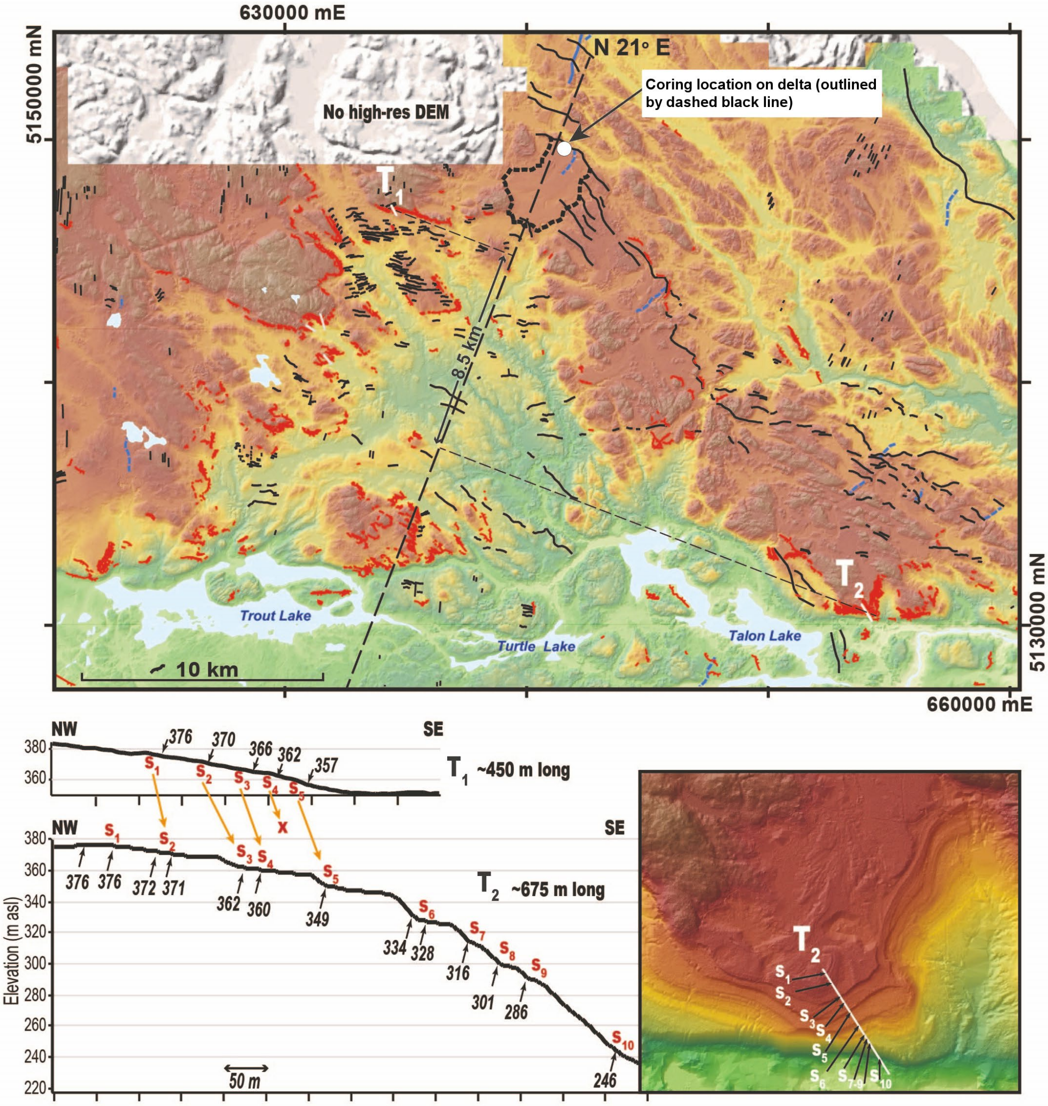

Figure 1b: Annotated DEM (MNRF 2016) showing the glacial features in the area immediately surrounding the coring location (white circle; *see* 1a for legend). Two transects (white lines; T1, T2) derived from digital data are highlighted and projected to the line of maximum uplift (N21°E; Karrow 2004). T1 shows five subtle shorelines (S1-S5), which are correlated to four of the ten shorelines on T2 (S2-S5), based on the magnitude of uplift along the 8.5km separating the two transect areas. Inset map shows the level of detail within the 2x2m (cell size) DEM in the local area. Vertical scale on transects is in metres above sea level (asl), horizontal scale divided into 50m increments (image: R. Mulligan).

Figure 2: Looking towards the north-west end of the kettle across the shallow pool that remained on the lake-bed in late summer 2010 and from where cores were extracted (photograph: R. Rabett).

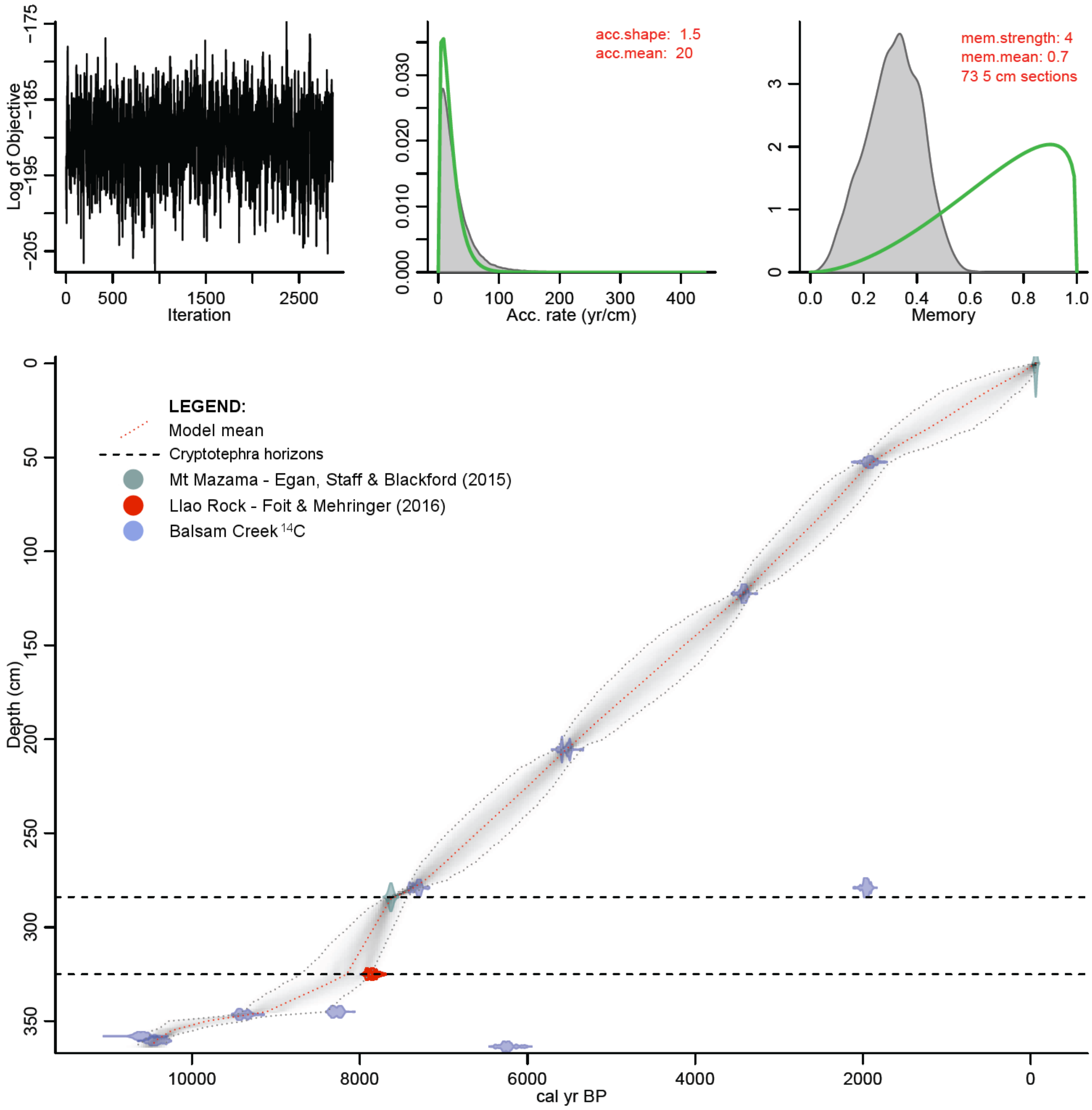

Figure 3: Balsam Creek age-depth curve, including independent dates for the Mt Mazama (Egan, Staff & Blackford 2015) and Llao Rock (Foit & Mehringer 2016) eruptions. The dashed black lines indicate depths where cryptotephra was identified within the Balsam Creek profile (284cm & 325cm) (histogram: M. Blaauw).

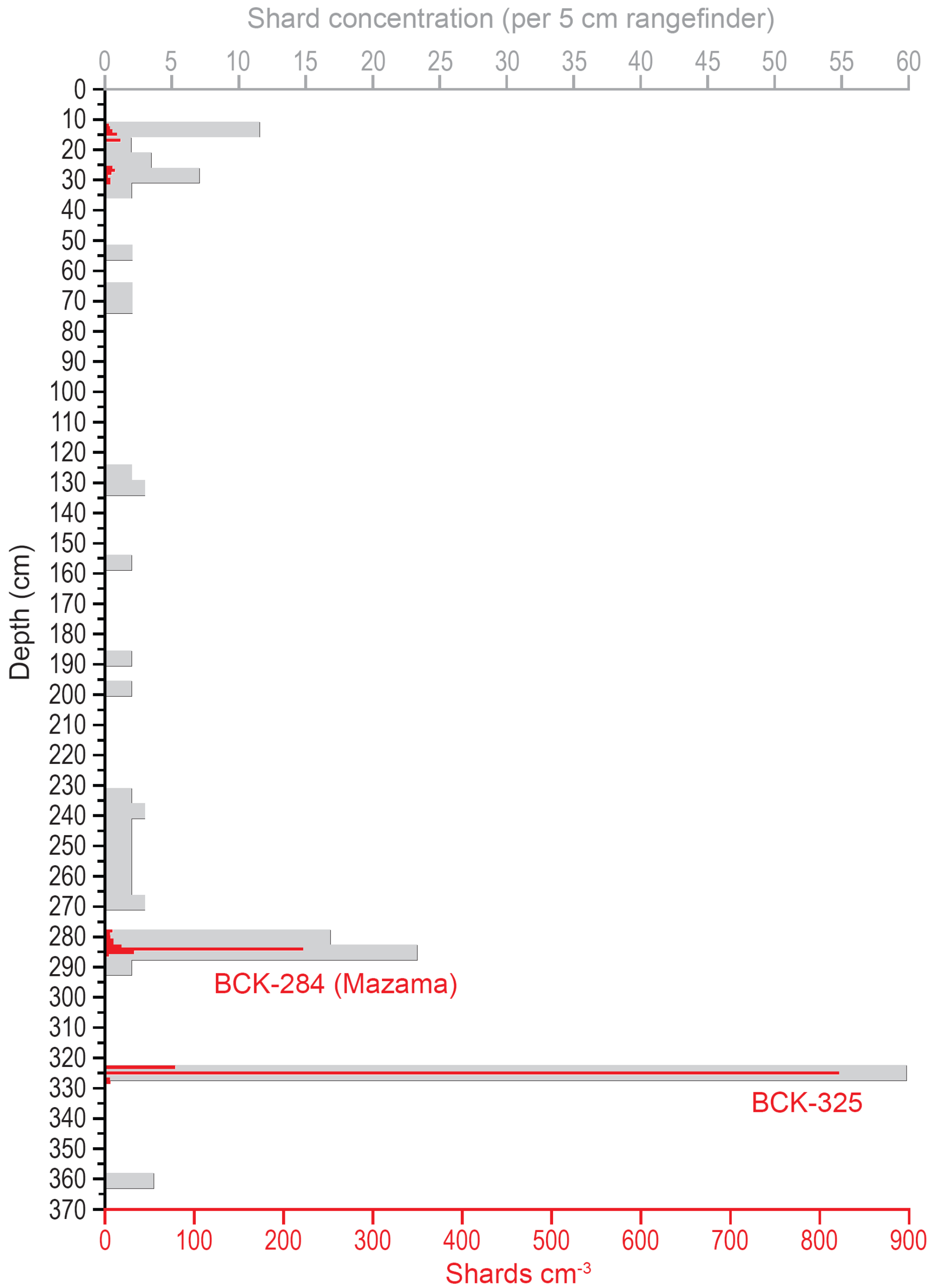

Figure 4: Tephrostratigraphy of Balsam Creek showing cryptotephra glass shard concentrations per 5cm rangefinder (grey) and cm^{-3} (red). The cryptotephra layer at 284-285cm (BCK-284) correlates to the Mazama ash, while the 325-326cm (BCK-325) cryptotephra is designated as an uncorrelated Mazama-like layer (data & presentation: S. Pyne-O'Donnell).

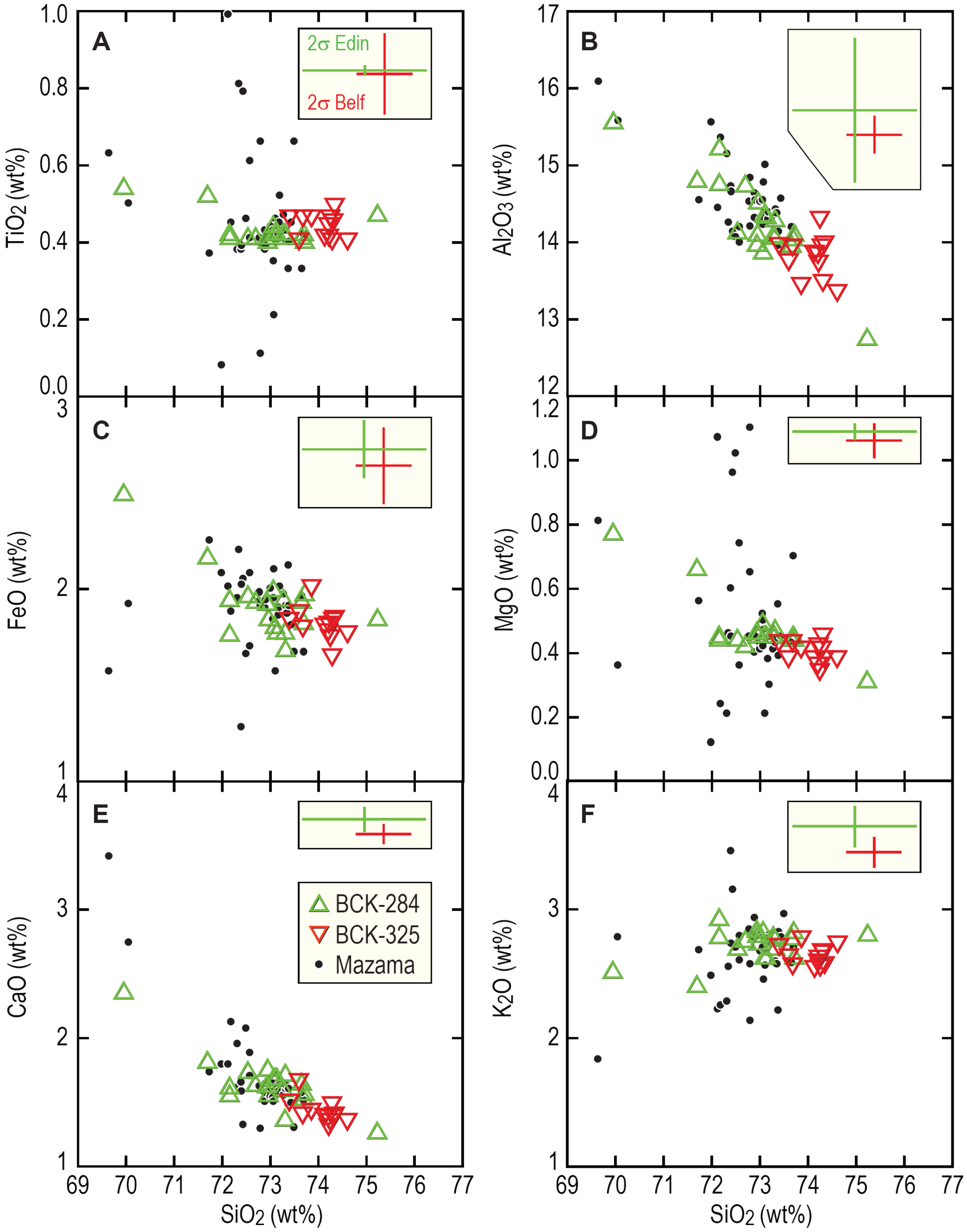

Figure 5: Element oxide biplots (wt%) for glass from cryptotephra layers BCK-284 and BCK-325 at Balsam Creek. In each case SiO2 is compared against **A:** TiO_2, **B:** Al_2O_3, **C:** FeO, **D:** MgO, **E:** CaO, **F:** K_2O. The Mazama ash reference (UA 1573) from Edmonton River Valley (Pyne-O'Donnell *et al*. 2012) is shown for correlation. Error bars shown are 2σ of the Lipari standard for the Belfast (red) and Edinburgh (green) microprobes. Note: All data points have been normalised for data set comparison. Supplementary Table 2 contains original un-normalised geochemical source data (data and presentation: S. Pyne-O'Donnell).

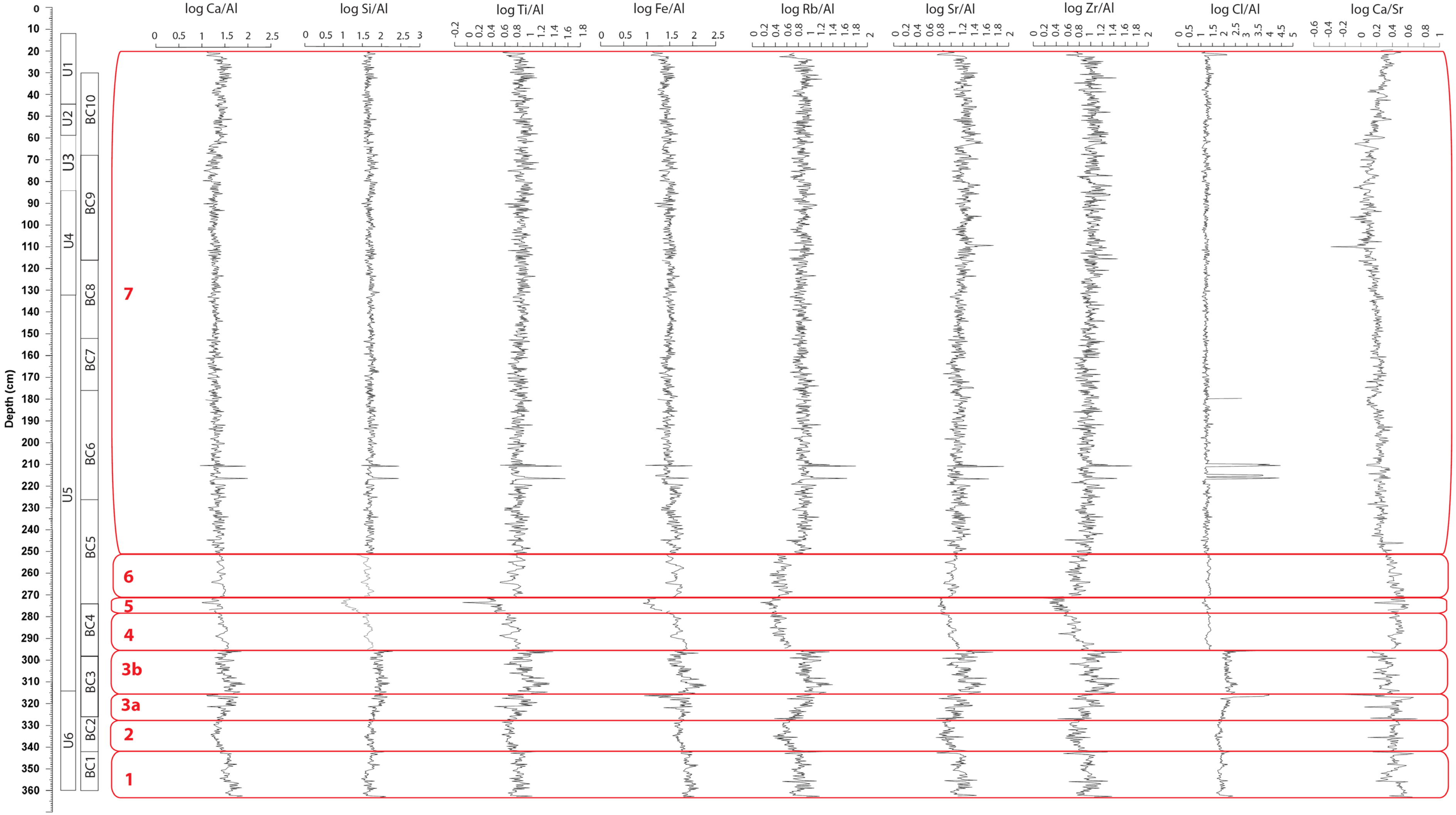

Figure 6: Chemozones 1-7 obtained from XRF analysis of the sediment profile. Element data is provided in counts per second (cps). The relationship between chemozones, pollen zones (BC) and sedimentary units (U) is presented against profile depth (data and presentation: L. Farr & S. Crowhurst).

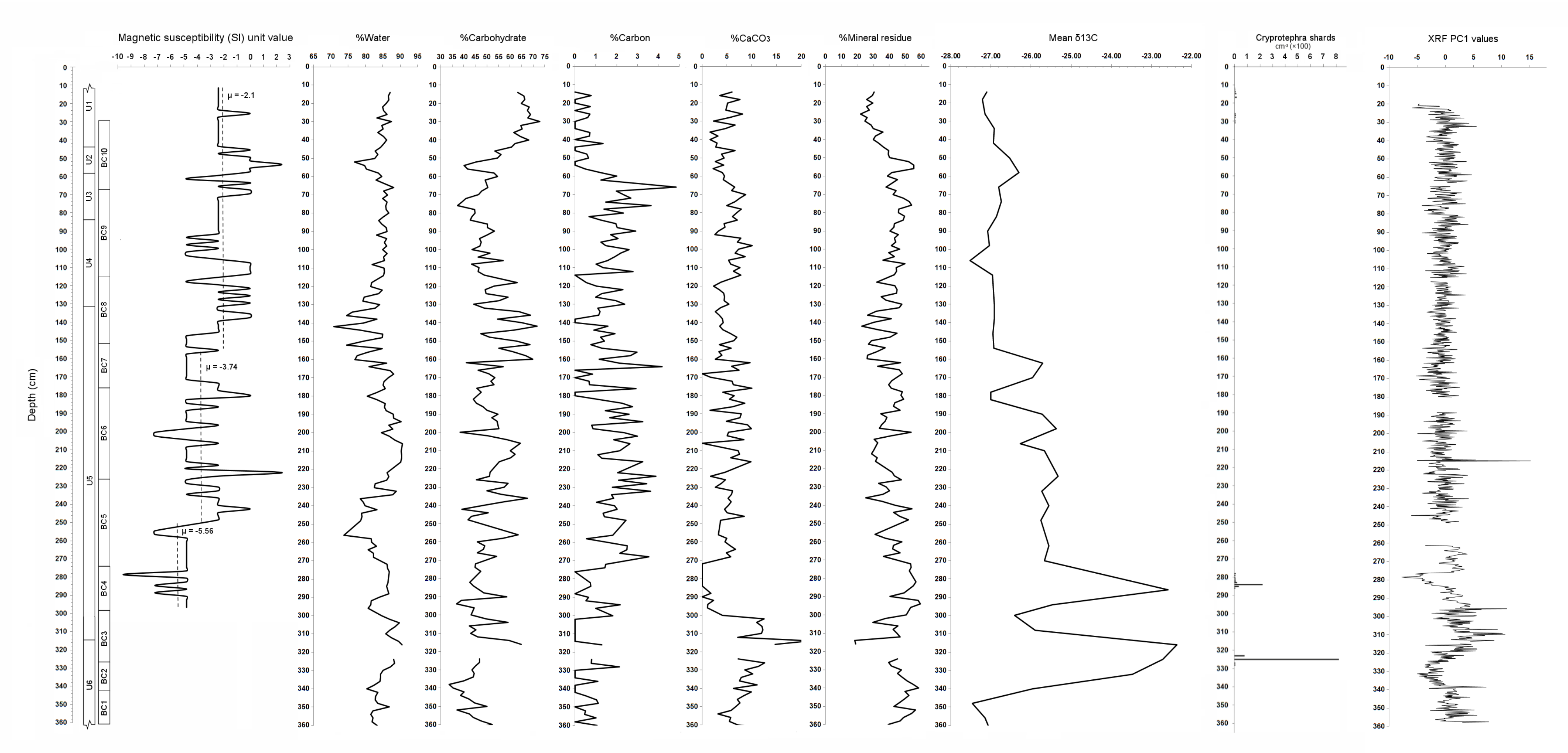

<< **Figure 7:** Compares data for magnetic susceptibility (including mean SI (μ) values), loss on ignition (% water then % dry weight), δ[13]C, cryptotephra shards and XRF PC1 values (20-357.75cm) from the Balsam Creek core. Pollen zones (BC) and sedimentary units (U) are provided for comparison (data: A. Pryor, L. Farr, S. Crowhurst, S. Pyne-O'Donnell, presentation: R. Rabett). >>

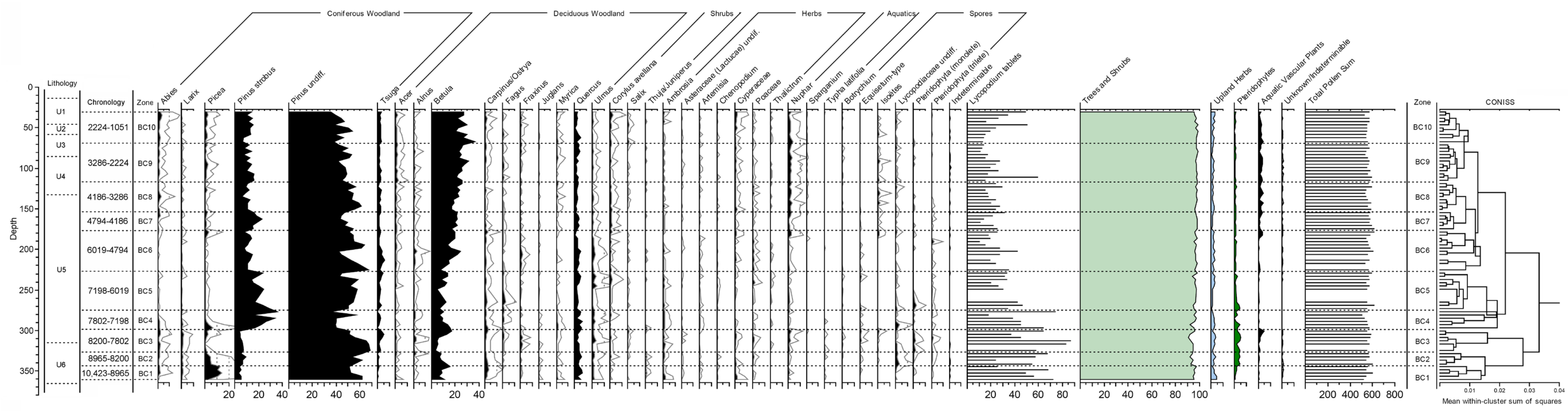

Figure 8: Tilia graph showing the pollen spectra from the Balsam Creek core, sedimentary units and age-depth modelled chronology (data and presentation: D. Simpson).

Table 1: Balsam Creek core, sedimentary unit (U) descriptions.

Depth (cm)	Description	Colour
12-44	**U1:** Organic macro-remains (leaves, small rootlets and other decaying plant matter) corresponding to modern detritus. Shrinkage in storage reduced upper core section length from 0-63cm (field measurement) to a 51cm section measuring 12-63cm.	Very dark brown (10YR 2/2)
44-59	**U2:** High % of decayed woody remains vs non-woody detritus, comprising frags up to *c*. 1cm. Sediments graded 1-2cm at the top of this unit into the overlying unit.	Dark reddish brown (5YR 3/2)
59-84	**U3:** Sharp transition from U2; contained more compacted sediment, lacking the decayed wood component of the overlying unit; two wood frags *c*. 4cm dia. at 78-75cm and 83-79cm.	Very dark brown (10YR 2/2)
84-132	**U4:** An increase in woody macro-remains relative to U3; included two large wood fragments at 95.5-93cm and 102.5-101cm.	Black (10YR 2/1)
132-314	**U5:** A single unit separated from U4 through decreasing size of macro-remains and organic detritus, which becomes more highly degraded with depth. Large woody frags: 277.5-271.5cm, 209-207cm, 203-199cm and 207-209cm.	Black (5YR 2.5/1)
314-363	**U6:** 4 oscillations (8 contexts) characterised by clay-rich sediment, with clear laminations (separating clayey and more silty lenses <5mm thick of fine highly degraded organic detritus), alternating with massive organic-rich horizons containing a high % of large and better preserved woody and non-woody macro-remains. The divisions between the sediment bands are sharp, suggesting rapid changes between the two sedimentary regimes.	Very dark greyish brown (10YR 3/2)

Table 2: ^{14}C dates obtained for the Balsam Creek core. All dates were processed through the AMS facility of the 14Chrono Centre, Queen's University Belfast.

Lab code	Sample (cm)	Material	AMS $\delta^{13}C$	^{14}C	±	IntCal13 (2σ)
UBA-22771	52-53	Wood	-29.6	1967	48	2010-1818
UBA-22772	121-124	Wood	-24.6	3202	34	3726-3575
UBA-22773	205-206	Wood	-25.8	4826	36	5553-5472
UBA-18803	278-280	Wood	-30.5	6376	36	7343-7254
UBA-22774	278-280	Wood	-23.7	2012	27	2007-1891
UBA-25525	345	Juv. *Carya* spp. nut	-	7464	44	8371-8191
UBA-22775	345-348	Seeds + plant macros	-23.7	8376	50	9497-9274
UBA-22776	357-359	Grass	-13.9	9371	53	10,732-10,485
UBA-27249	360-361	Terrestrial plant macros	-	9260	41	10,562-10,288
UBA-25526	363-364	Gymnosperm leaf + plant macros	-	5452	64	6399-6173

Table 3: Descriptions of discrete chemozones (CZ) within the Balsam Creek core.

Depth (cm)	Description
20-251	**CZ7:** Low-amplitude changes in Ca/Al, Ti/Al, Fe/Al and Sr/Al are observed in this chemozone, and show well-defined co-variability. Ca/Sr ratio values show an independent trend that is sometimes inversely related to the Ca/Al, Ti/Al, Fe/Al and Sr/Al trend. The Ca/Sr values in CZ7 appear to show some degree of correlation to the $\delta^{13}C$ oscillations observed, at the same depths, in $\delta^{13}C$ 'Zone E'. Cl/Al show little variation apart from two pronounced peaks at 211cm and 216cm; these are observed in all ratio datasets where aluminium is used. Ca/Sr ratio values increase between 63cm and 20cm.
251-271	**CZ6:** Moderate amplitude, co-variable oscillations in the Ca/Al, Si/al, Ti/A, Fe/Al, Rb/Al, Sr/Al, and Zr/Al data series characterise CZ6.
271-278	**CZ5:** A large single piece of wood defines the depth parameters of this chemozone. Minima values are observed for Si/Al, Ti/Al, Fe/Al and Zr/Al. A significant, synchronous, abrupt decline in Ti/Al and Ca/Sr values is observed at 274cm.
277-295	**CZ4:** Within this chemozone, Ca/Al, Si/Al, Ti/Al and Fe/Al ratios are closely related, and share very similar peak-trough profiles. Rb/Al, Sr/Al and Zr/Al values show an overall trend of decline. Cl/Al ratios drop abruptly to from values of 2 to *c*. 1.2 (this amplitude continues throughout the remainder of the core).

296-316	**CZ3b:** Chemozone 3 contains a series of 7–8 sharp peaks and troughs in the Ca/Al, Ti/Al, Rb/Al, Sr/Al and Zr/Al ratio values. The Rb/Al ratio values show minor oscillations which do not share the same signature as the other detrital ratios. In C3b, Ca/Sr ratios have an inverse relationship to (Ca/Al and Zr/Al). The boundary between Chemozone BC3a and BC3b is marked by a distinct peak in the Cl/Al values which may relate to the marine influence and the 8.2 cal. BP Cold Event.
316-328	**CZ3a:** In this chemozone Ca/Sr ratio values exhibit a peak and trough pattern which synchronously correlates with ratios (Ca/Al and Zr/Al).
328-342	**CZ2:** This chemozone is characterised by a 'U'-shaped decline in Ca/Al, Rb/Al, Sr/Al and Zr/Al ratios. Si/Ti, Ti/Al and Fe/Al values show lower amplitude, synchronous change.
342-363	**CZ1:** A peak-trough-peak curve in Ca/Al and Ca/Sr values characterise this chemozone. Rb/Al, Sr/Al and Zr/Al ratios have closely related and synchronous peak-trough-peak pattern, which is characterised by acute oscillations.

Supplementary Table 1: Balsam Creek age-depth model output using *Bacon*, incorporating all Balsam Creek dates (this study, Table 2) and published dates for the Mount Mazama and Llao Rock volcanic eruptions from Egan, Staff & Blackford (2015) and Foit & Mehringer (2016), respectively.

Depth	Max	Min	Median	Mean	Depth	Max	Min	Median	Mean	Depth	Max	Min	Median	Mean
0	-29	-86	-59	-59	122	3547	3306	3415	3420	244	6816	6093	6465	6460
1	50	-71	-30	-25	123	3572	3331	3438	3444	245	6850	6107	6487	6484
2	156	-65	-4	9	124	3613	3354	3460	3467	246	6862	6141	6513	6509
3	259	-59	23	43	125	3658	3368	3480	3491	247	6879	6165	6536	6534
4	361	-55	50	77	126	3688	3390	3505	3517	248	6904	6188	6563	6558
5	465	-51	77	111	127	3729	3402	3532	3542	249	6933	6201	6587	6583
6	502	-24	121	154	128	3779	3412	3555	3568	250	6966	6219	6613	6608
7	566	-8	169	197	129	3840	3419	3579	3594	251	6979	6254	6636	6632
8	635	3	211	239	130	3914	3426	3599	3619	252	6997	6275	6662	6655
9	719	15	250	282	131	3932	3448	3626	3645	253	7019	6300	6687	6679
10	803	23	291	325	132	3967	3464	3652	3671	254	7039	6324	6710	6703
11	842	56	332	364	133	4006	3474	3679	3696	255	7069	6338	6735	6727

12	878	82	376	403	134	4050	3485	3704	3722	256	7081	6383	6758	6752
13	931	101	420	442	135	4105	3496	3729	3748	257	7098	6416	6783	6777
14	1002	117	457	480	136	4123	3520	3756	3773	258	7113	6439	6810	6802
15	1069	129	491	519	137	4150	3540	3781	3797	259	7137	6460	6837	6827
16	1092	174	525	556	138	4185	3554	3805	3822	260	7160	6477	6860	6851
17	1115	209	567	592	139	4225	3567	3830	3847	261	7171	6510	6885	6875
18	1149	231	605	629	140	4278	3578	3852	3872	262	7184	6544	6910	6898
19	1184	252	650	665	141	4308	3609	3876	3898	263	7202	6568	6933	6922
20	1236	270	690	702	142	4337	3630	3904	3923	264	7230	6587	6957	6945
21	1253	305	727	737	143	4368	3645	3930	3949	265	7258	6603	6982	6968
22	1276	320	764	772	144	4403	3662	3957	3974	266	7266	6642	7007	6994
23	1300	342	806	807	145	4438	3676	3984	4000	267	7277	6686	7033	7019
24	1340	363	843	842	146	4456	3703	4014	4027	268	7289	6719	7059	7045
25	1394	384	882	877	147	4481	3724	4042	4054	269	7307	6745	7087	7071
26	1415	422	916	912	148	4503	3739	4070	4081	270	7330	6765	7112	7096
27	1436	453	950	947	149	4541	3756	4098	4108	271	7339	6822	7137	7122
28	1464	471	985	982	150	4582	3767	4122	4134	272	7346	6871	7162	7147
29	1492	497	1020	1016	151	4600	3800	4150	4160	273	7358	6906	7188	7173
30	1528	519	1058	1051	152	4620	3824	4172	4186	274	7371	6938	7215	7198
31	1549	574	1092	1088	153	4640	3843	4198	4211	275	7388	6955	7241	7223
32	1572	605	1131	1125	154	4667	3857	4225	4237	276	7396	7044	7269	7257
33	1601	651	1166	1161	155	4694	3871	4251	4262	277	7404	7128	7298	7291
34	1628	669	1206	1198	156	4716	3889	4275	4287	278	7416	7192	7332	7324
35	1667	680	1248	1235	157	4737	3907	4303	4312	279	7441	7252	7369	7358
36	1682	764	1286	1276	158	4766	3925	4327	4336	280	7503	7270	7399	7391
37	1696	840	1329	1317	159	4803	3946	4353	4361	281	7529	7331	7445	7439
38	1711	896	1372	1358	160	4827	3965	4380	4386	282	7562	7383	7492	7486
39	1742	934	1419	1399	161	4848	4000	4406	4411	283	7607	7409	7543	7534
40	1782	961	1460	1440	162	4866	4028	4433	4437	284	7662	7428	7593	7582
41	1793	1029	1498	1478	163	4886	4048	4459	4462	285	7732	7445	7642	7629
42	1810	1094	1539	1515	164	4910	4073	4484	4488	286	7753	7458	7655	7643

43	1833	1144	1577	1553	165	4938	4094	4511	4513	287	7781	7469	7666	7657
44	1857	1192	1617	1590	166	4957	4125	4535	4538	288	7818	7479	7678	7670
45	1895	1236	1653	1628	167	4981	4147	4560	4563	289	7855	7485	7687	7684
46	1907	1332	1684	1664	168	5001	4175	4584	4588	290	7898	7496	7697	7698
47	1919	1408	1714	1699	169	5029	4192	4610	4613	291	7919	7506	7710	7711
48	1932	1485	1747	1735	170	5061	4207	4637	4638	292	7942	7520	7722	7724
49	1952	1535	1783	1771	171	5076	4243	4660	4664	293	7967	7528	7734	7737
50	1981	1568	1818	1807	172	5093	4281	4687	4690	294	7998	7537	7744	7751
51	1996	1614	1846	1836	173	5114	4312	4715	4716	295	8025	7543	7755	7764
52	2015	1652	1876	1865	174	5143	4328	4743	4742	296	8044	7554	7768	7777
53	2045	1682	1905	1894	175	5170	4347	4776	4768	297	8064	7565	7780	7790
54	2094	1710	1930	1922	176	5185	4385	4798	4794	298	8085	7579	7791	7802
55	2162	1732	1953	1951	177	5199	4419	4824	4821	299	8111	7590	7802	7815
56	2181	1752	1975	1973	178	5215	4449	4852	4847	300	8142	7598	7813	7828
57	2211	1770	1996	1995	179	5231	4468	4881	4873	301	8156	7611	7826	7842
58	2251	1785	2016	2017	180	5260	4495	4907	4900	302	8181	7620	7840	7855
59	2292	1799	2035	2039	181	5274	4538	4932	4925	303	8203	7631	7852	7868
60	2341	1808	2051	2060	182	5291	4575	4959	4950	304	8236	7639	7864	7881
61	2356	1828	2073	2081	183	5307	4608	4987	4975	305	8263	7648	7874	7894
62	2387	1848	2095	2102	184	5325	4627	5012	5000	306	8281	7662	7887	7907
63	2411	1868	2117	2122	185	5357	4649	5037	5025	307	8299	7674	7899	7920
64	2443	1884	2135	2143	186	5371	4688	5063	5051	308	8330	7686	7912	7933
65	2480	1895	2154	2164	187	5389	4726	5088	5077	309	8352	7694	7924	7946
66	2497	1916	2177	2184	188	5408	4753	5114	5103	310	8377	7699	7936	7958
67	2521	1930	2200	2204	189	5429	4780	5144	5128	311	8396	7713	7949	7972
68	2540	1945	2219	2224	190	5454	4801	5170	5154	312	8411	7728	7962	7985
69	2568	1959	2239	2244	191	5462	4836	5193	5178	313	8429	7737	7976	7998
70	2598	1971	2259	2264	192	5474	4866	5217	5202	314	8449	7750	7989	8012
71	2614	1995	2281	2285	193	5488	4891	5239	5227	315	8463	7758	8002	8025
72	2632	2013	2304	2307	194	5504	4916	5264	5251	316	8484	7768	8019	8038
73	2656	2033	2324	2328	195	5523	4933	5291	5275	317	8512	7781	8033	8051

74	2680	2050	2346	2350	196	5534	4972	5314	5299	318	8539	7790	8046	8065
75	2709	2068	2367	2371	197	5547	5011	5338	5323	319	8563	7801	8061	8078
76	2725	2095	2388	2393	198	5558	5045	5364	5347	320	8586	7809	8074	8091
77	2741	2120	2410	2415	199	5572	5069	5389	5371	321	8608	7824	8086	8104
78	2758	2133	2435	2437	200	5593	5089	5414	5395	322	8636	7835	8099	8117
79	2777	2144	2457	2459	201	5601	5159	5435	5422	323	8656	7848	8111	8130
80	2801	2158	2480	2481	202	5614	5235	5455	5449	324	8680	7859	8124	8142
81	2814	2185	2501	2502	203	5624	5292	5475	5476	325	8711	7866	8138	8155
82	2829	2209	2521	2523	204	5642	5324	5500	5503	326	8737	7907	8179	8200
83	2852	2232	2542	2544	205	5666	5342	5523	5531	327	8778	7928	8223	8244
84	2878	2256	2565	2565	206	5689	5370	5546	5553	328	8815	7946	8272	8288
85	2904	2265	2586	2586	207	5732	5389	5574	5576	329	8865	7958	8318	8332
86	2918	2297	2609	2609	208	5777	5406	5598	5598	330	8915	7970	8362	8377
87	2936	2323	2634	2633	209	5833	5418	5615	5621	331	8939	8010	8412	8426
88	2959	2341	2659	2656	210	5888	5433	5633	5643	332	8967	8042	8465	8474
89	2990	2357	2682	2679	211	5914	5459	5657	5667	333	9005	8067	8515	8523
90	3026	2371	2705	2702	212	5940	5478	5682	5690	334	9046	8094	8570	8572
91	3038	2397	2728	2725	213	5980	5500	5704	5714	335	9106	8116	8621	8621
92	3051	2421	2751	2747	214	6028	5518	5725	5738	336	9135	8172	8671	8671
93	3069	2443	2772	2769	215	6087	5530	5747	5761	337	9162	8204	8725	8720
94	3087	2465	2795	2792	216	6114	5551	5771	5785	338	9189	8229	8776	8769
95	3115	2483	2818	2814	217	6129	5566	5796	5808	339	9229	8246	8829	8819
96	3130	2516	2839	2836	218	6151	5580	5821	5831	340	9282	8264	8886	8868
97	3150	2545	2864	2859	219	6186	5596	5843	5854	341	9300	8303	8932	8917
98	3170	2567	2886	2882	220	6223	5609	5864	5877	342	9312	8331	8982	8965
99	3195	2583	2910	2904	221	6241	5633	5889	5901	343	9338	8349	9044	9014
100	3213	2600	2932	2927	222	6265	5650	5914	5924	344	9363	8364	9103	9062
101	3227	2637	2957	2950	223	6286	5663	5939	5948	345	9403	8387	9162	9111
102	3242	2668	2982	2974	224	6318	5677	5962	5971	346	9447	8694	9289	9255
103	3261	2695	3007	2997	225	6354	5690	5985	5994	347	9570	9006	9425	9399
104	3286	2721	3032	3021	226	6371	5717	6008	6019	348	9777	9205	9559	9543

105	3311	2740	3054	3044	227	6388	5737	6035	6044	349	10023	9316	9692	9687
106	3320	2772	3075	3067	228	6422	5754	6061	6068	350	10290	9373	9831	9831
107	3331	2809	3098	3089	229	6448	5767	6086	6093	351	10308	9537	9912	9913
108	3347	2831	3121	3111	230	6483	5777	6113	6118	352	10332	9682	9991	9996
109	3361	2858	3146	3134	231	6501	5811	6135	6142	353	10364	9813	10074	10078
110	3386	2877	3168	3156	232	6528	5842	6161	6166	354	10399	9912	10163	10161
111	3396	2913	3187	3178	233	6550	5857	6181	6190	355	10474	9981	10246	10243
112	3408	2942	3210	3199	234	6576	5867	6207	6214	356	10486	10082	10273	10279
113	3420	2967	3234	3221	235	6617	5879	6232	6238	357	10498	10168	10302	10315
114	3435	2991	3254	3243	236	6630	5915	6258	6262	358	10514	10232	10339	10351
115	3454	3016	3277	3264	237	6641	5936	6283	6287	359	10537	10263	10383	10387
116	3464	3072	3295	3286	238	6676	5960	6310	6312	360	10564	10284	10426	10423
117	3476	3119	3315	3308	239	6699	5985	6338	6337	361	10586	10302	10446	10443
118	3487	3165	3334	3330	240	6730	6000	6361	6362	362	10622	10313	10464	10462
119	3505	3196	3355	3352	241	6749	6036	6386	6386	363	10669	10322	10483	10482
120	3523	3216	3377	3373	242	6767	6060	6413	6411					
121	3533	3266	3394	3397	243	6788	6080	6438	6435					

Supplementary Table 2: Element oxide concentrations (original un-normalised wt%) of single glass shards from Balsam Creek cryptotephra layers analysed at Queen's University Belfast (BCK-325) and Edinburgh University (BCK-284). Mean and one standard deviation (1σ) are also shown, with total iron expressed as FeO. *n* = number of analyses.

n	SiO_2	TiO_2	Al_2O_3	FeO	MnO	MgO	CaO	Na_2O	K_2O	P_2O_5	Cl	F	Total
Queen's University Belfast (January 2016)													
Balsam Creek (BCK-325) cryptotephra													
1	69.53	0.39	13.02	1.79	0.10	0.37	1.59	5.02	2.50		0.19		*94.48*
2	69.79	0.45	13.30	1.76	-0.01	0.42	1.45	5.11	2.60		0.22		95.10
3	70.49	0.45	13.37	1.73	0.15	0.42	1.36	5.04	2.47		0.19		95.68
4	70.50	0.45	12.86	1.93	0.07	0.40	1.38	5.03	2.66		0.20		95.47
5	70.84	0.40	13.27	1.74	-0.07	0.37	1.35	4.97	2.45		0.25		95.57

n	SiO_2	TiO_2	Al_2O_3	FeO	MnO	MgO	CaO	Na_2O	K_2O	P_2O_5	Cl	F	Total
6	70.94	0.45	13.69	1.68	0.03	0.33	1.31	4.49	2.46		0.17		95.55
7	71.21	0.39	13.39	1.59	0.15	0.40	1.44	4.51	2.58		0.20		95.87
8	71.34	0.43	13.33	1.72	0.06	0.36	1.35	4.85	2.51		0.19		96.14
9	71.37	0.39	12.80	1.70	0.03	0.37	1.31	4.89	2.63		0.17		95.67
10	71.46	0.44	12.99	1.78	0.11	0.44	1.35	4.82	2.58		0.21		96.18
11	71.46	0.40	13.25	1.76	-0.03	0.41	1.28	5.04	2.54		0.19		96.30
12	72.28	0.49	13.62	1.81	0.02	0.38	1.38	4.48	2.52		0.25		97.24
Mean	**70.93**	**0.43**	**13.24**	**1.75**	**0.05**	**0.39**	**1.38**	**4.85**	**2.54**		**0.20**		**95.77**
1σ	**0.77**	**0.03**	**0.28**	**0.08**	**0.07**	**0.03**	**0.08**	**0.23**	**0.07**		**0.03**		**0.68**
Belfast Lipari secondary standard													
	75.16	0.00	12.40	1.38	0.03	0.01	0.63	3.12	4.86		0.30		97.88
	75.02	0.03	12.48	1.42	0.06	0.00	0.68	3.06	4.94		0.32		98.00
	74.90	0.16	12.20	1.47	0.04	0.01	0.66	3.19	5.10		0.29		98.03
	75.46	-0.03	12.30	1.32	0.17	-0.04	0.63	3.08	4.93		0.33		98.15
	75.47	0.09	12.51	1.40	0.10	0.01	0.62	2.86	4.94		0.28		98.26
	75.61	0.08	12.44	1.58	-0.05	-0.02	0.66	2.88	4.89		0.36		98.42
	75.73	0.07	12.27	1.36	0.06	-0.01	0.66	3.03	4.91		0.37		98.45
	75.80	0.08	12.48	1.47	0.01	-0.01	0.56	3.01	4.93		0.27		98.62
	75.12	0.05	12.43	1.49	0.11	0.05	0.61	3.66	4.88		0.33		98.73
	75.31	0.05	12.53	1.58	-0.02	0.02	0.63	3.54	4.92		0.33		98.88
	75.17	0.08	12.42	1.61	0.08	0.03	0.66	3.97	4.96		0.33		99.31
	75.51	0.14	12.65	1.59	0.04	0.05	0.56	3.66	4.94		0.29		99.43

n	SiO_2	TiO_2	Al_2O_3	FeO	MnO	MgO	CaO	Na_2O	K_2O	P_2O_5	Cl	F	Total
							Edinburgh University (May 2018)						
Balsam Creek (BCK-284) cryptotephra (Correlation: Mazama ash)													
1	70.50	0.42	13.38	1.92	0.04	0.47	1.61	5.31	2.72	0.06	0.12	0.08	96.64
2	71.71	0.41	13.65	1.77	0.04	0.44	1.48	4.92	2.75	0.06	0.14	0.04	97.42
3	73.49	0.46	12.44	1.80	0.04	0.31	1.23	5.05	2.73	0.07	0.14	0.01	97.78
4	72.20	0.41	13.68	1.89	0.05	0.43	1.61	4.92	2.72	0.07	0.14	0.06	98.16

n	SiO_2	TiO_2	Al_2O_3	FeO	MnO	MgO	CaO	Na_2O	K_2O	P_2O_5	Cl	F	Total
5	72.26	0.42	13.85	1.75	0.05	0.45	1.34	5.61	2.72	0.06	0.14	0.04	98.68
6	72.06	0.41	14.03	1.95	0.06	0.43	1.72	5.87	2.67	0.06	0.15	0.02	99.43
7	72.68	0.42	14.24	1.76	0.05	0.44	1.67	5.41	2.60	0.04	0.12	0.06	99.49
8	73.30	0.40	14.01	1.96	0.05	0.43	1.55	4.99	2.61	0.06	0.13	0.06	99.56
9	72.80	0.42	14.29	1.80	0.05	0.45	1.67	5.36	2.61	0.06	0.15	0.05	99.70
10	72.67	0.40	14.04	1.91	0.06	0.46	1.75	5.43	2.78	0.06	0.14	0.09	99.78
11	71.42	0.52	14.73	2.15	0.07	0.66	1.80	5.75	2.39	0.12	0.13	0.05	99.79
12	72.02	0.42	15.18	1.93	0.04	0.44	1.61	5.25	2.78	0.07	0.14	0.06	99.95
13	73.34	0.42	14.08	1.94	0.06	0.45	1.59	5.27	2.78	0.07	0.15	0.04	100.20
14	72.79	0.41	14.75	1.94	0.05	0.42	1.64	5.27	2.76	0.06	0.13	0.00	100.21
15	73.01	0.41	14.52	1.84	0.05	0.45	1.55	5.36	2.73	0.08	0.14	0.06	100.21
16	70.35	0.55	15.64	2.51	0.07	0.77	2.36	5.63	2.53	0.11	0.17	0.07	100.75
17	73.82	0.41	14.38	1.70	0.05	0.48	1.72	5.28	2.71	0.07	0.14	0.00	100.77
18	73.44	0.41	14.06	1.93	0.07	0.46	1.63	5.72	2.85	0.06	0.13	0.06	100.84
19	72.87	0.42	14.90	1.77	0.05	0.46	1.57	5.87	2.95	0.07	0.14	0.03	101.09
Mean	**72.46**	**0.43**	**14.20**	**1.91**	**0.05**	**0.47**	**1.64**	**5.38**	**2.71**	**0.07**	**0.14**	**0.05**	**99.50**
1σ	**0.96**	**0.04**	**0.70**	**0.18**	**0.01**	**0.10**	**0.22**	**0.30**	**0.12**	**0.02**	**0.01**	**0.03**	**1.23**
Edinburgh Lipari secondary standard													
22/05/18													
08:04:25	74.10	0.08	12.95	1.48	0.07	0.02	0.79	4.51	5.05	0.00	0.28	0.16	99.50
08:12:12	74.96	0.08	13.20	1.65	0.07	0.05	0.76	4.21	5.04	0.02	0.29	0.12	100.45
08:19:56	74.09	0.08	12.27	1.52	0.08	0.02	0.66	4.16	5.16	0.00	0.29	0.11	98.45
23/05/18													
08:13:48	75.61	0.08	12.77	1.58	0.06	0.05	0.78	4.07	5.17	0.00	0.25	0.08	100.52
08:21:43	75.30	0.07	12.81	1.63	0.06	0.03	0.76	4.16	5.11	0.01	0.26	0.14	100.35
08:29:39	75.02	0.07	13.21	1.57	0.07	0.04	0.74	4.21	5.13	0.00	0.25	0.10	100.42
08:37:34	75.56	0.07	11.98	1.45	0.07	0.04	0.73	4.11	5.26	0.01	0.24	0.11	99.64